THE UNIVERSITY OF QUEENSLAND

Phase Equilibrium Study of Cyclopentane Hydrates in Brine

Student Name: Yuanyuan, YUAN

Course Code: ENGG7282

Supervisor: Dr. Liguang Wang

Submission date: 30 May 2019

Abstract

Natural gas gradually becomes one of the major energy resources in the world. Due to the growing demand for energy consumption and increasing environmental concern, natural gas has an optimistic future market especially compared with other fossil fuels. The issue for utilizing natural gas broadly is that the difficulties exist in transport and storage since the proven natural gas reserves are dispersedly distributed over the world. High-cost and high-risk gaseous or liquified natural gas transport and storage limited the global application of natural gas.

In this project, the liquid hydrocarbon, cyclopentane, was selected for the hydrate formation and dissociation experiment since its hydrate structure is the same as natural hydrate structure but can be easily formed under near ambient conditions. Three types of salt solutions, sodium chloride (NaCl), calcium chloride ($CaCl_2$), and aluminium chloride ($AlCl_3$) solutions in different molality concentrations were prepared. The formation experiment was conducted by cooling down the mixture of cyclopentane and salt solution in a cryostat at atmospheric pressure. Temperature probes were placed in the solution phase. The dissociation experiment started when sufficient hydrates formed. A quick dissociation method was applied to the cyclopentane phase equilibrium temperature measurement. The experimental phenomena and equilibrium temperature were observed visually.

The phase equilibrium temperature data for cyclopentane hydrates were measured from the experiment. The collected data were progressed and plotted over the concentrations (mass fraction, molality, effective mole fraction, and ionic strength). Possible relationships were proposed and analysed. In addition, some preliminary experiments had been conducted to obtain supporting information and data. Hydrate formation rate was improved by increasing subcooling and introducing agitation. In this thesis, the phenomena of cyclopentane hydrate formation and dissociation had also been observed visually during the experiments.

The equilibrium temperatures gathered from this thesis can be applied for further studies. A slower dissociation method can be used to obtain the equilibrium data with high accuracy. Furthermore, the reliable data may be applied for relationship studies on cyclopentane hydrate nucleation rate and effective mole fraction in electrolytes under the same subcooling level.

Keywords:

Cyclopentane hydrate, hydrate formation, hydrate dissociation, phase equilibrium temperature, brine, molality, effective mole fraction

Acknowledgments

First of all, I would give my gratitude to my supervisor, Dr. Liguang Wang, for his guidance and support on my research project and comments and suggestions on my thesis.

I would like to thank Dr. Hangil Park, who helped me to start my laboratory work and provided support during the project.

I would also give thanks to my parents and friends for their encouragement and support.

Table of Contents

List of Figures

List of Tables

List of Equations

List of Abbreviations

$AlCl_3$	Aluminium Chloride
a_w	Water Activity
C_2H_5OH	Ethanol
C_3H_8	Propane
$CaCl_2$	Calcium Chloride
$C\text{-}C_3H_6$	Cyclopropane
CH_4	Methane
CNG	Compressed Natural Gas
CO_2	Carbon Dioxide
CP	Cyclopentane
CuO	Cupric Oxide
DI water	Deionized Water
Fe_3O_4	Iron(II,III) Oxide
KOH	Potassium Hydroxide
LNG	Liquefied Natural Gas
N_2	Nitrogen
NaCl	Sodium Chloride
$n\text{-}C_4H_{10}$	n-Butane
NO_x	Nitrogen Oxides
O_2	Oxygen
SDS	Sodium Dodecyl Sulfate
sH	Structure H
sI	Structure I
sII	Structure II
SL	Sulfonated Lignin
SNG	Solidified Natural Gas
SO_2	Sulfur Dioxide
STP	Standard Temperature and Pressure
THI	Thermodynamic Hydrate Inhibitor

Chapter 1: Introduction

Natural gas has become one of the essential energy resources in the world. The latest data, which is provided by Our World In Data[1-3], shows the broad distribution of proven reserves and their high capacities over the world (figure attached in APPENDIX-A). The data supported the prospection of natural gas development. As a cheap, clean and high-efficient energy, natural gas gradually replaces the position of other fossil fuels, such as coal and petroleum, at the end-users[4]. Especially, the increasing environmental concerns also facilitate the demand for natural gas[5]. Therefore, the studies on improving advanced techniques for natural gas mining, transportation, and storage are necessary to meet the rapid growth of natural gas utilization.

Gas hydrates are the ice-like crystalline solids which consist of water and guest gas, such as carbon dioxide, methane, ethane, etc[6]. A large amount of gas can be packed by within the crystal, particularly 1 m^3 hydrate may contain approximately 150-180 m^3 methane under the standard temperature and pressure (STP) conditions[7]. Due to its high gas holdup ability, natural gas hydrate, also known as solidified natural gas (SNG), has been considered as an alternative transportation and storage option compared with liquefied natural gas (LNG) and compressed natural gas (CNG)[8], which can further promote the safety and convenience of natural gas transportation and storage and reduce the expenditure of corresponding processes[9].

To apply the natural gas hydrate technique to the real-world industry, a set of problems required to be solved. One of the most challenging issues is to improve the hydrate formation process so that it can be employed in large-scale production[10]. Relevant tasks need to be overcome, for example, accelerating hydrate formation speed, enhancing the final hydrate uptake, simplifying hydrate formation process, lowering the costs of hydrate formation technology, conforming to the idea of sustainability, etc. At present, the studies of clathrate hydrates are conducted mainly from two directions: thermodynamic and kinetics to understand the hydrate formation and dissociation processes.

Cyclopentane (CP) is used as a model system to study the natural gas hydrate since they have the same hydrate structures[11; 12]. The CP hydrate phase equilibrium temperature data in sodium chloride (NaCl) and calcium chloride ($CaCl_2$) solutions, particularly NaCl solution, have been investigated by other researchers., but limited data of aluminium chloride ($AlCl_3$) solution can be found.

This thesis aims to measure the phase equilibrium temperature of CP hydrate in different types of electrolytes at different concentrations. NaCl solution, $CaCl_2$ solution, and $AlCl_3$ solution are

prepared for this project. Also, the phenomena are observed visually during the CP hydrate formation and dissociation process and discussed in this thesis.

The main contents discussed in the following chapters are listed below:

Chapter 2 Literature Review: This chapter includes a review of the literature, the knowledge gaps in current literature, the research proposals and hypotheses.

Chapter 3 Experimental Apparatus and Methodology: This chapter discussed the experimental apparatus and materials, experimental processes for preliminary experiments and hydrate formation and dissociation experiments, and data progressing.

Chapter 4 Result Analyses and Discussions: This chapter gathered the results of the experiments, the analyses and discussions on the results are conducted.

Chapter 5 Conclusion and Future Works: This chapter summarized the main tasks and findings of the thesis; recommendations on future work and current experimental improvement are listed.

Chapter 2: Literature Review

2.1 Clathrate Hydrate

2.1.1 What is Clathrate Hydrate

Clathrate hydrate is a kind of ice-like crystalline solids which is formed with gas and water. Various guest gases[6], such as carbon dioxide, methane, and ethane, can be "captured" in the cavities of the "host" material water[13].

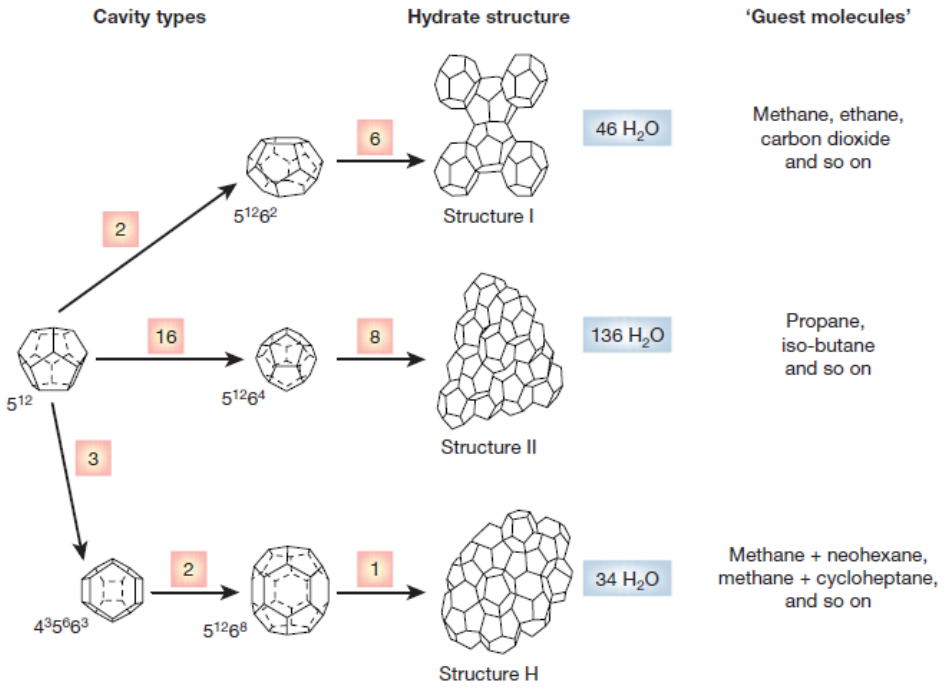

Figure 1 The Structure of per Unit Clathrate Hydrate (cites: Sloan, 2003, Figure 1)

Sloan[14] mentioned three common hydrate structures in his article which is cited in Figure 1. These structures are also identified as cubic structure I (sI), cubic structure II (sII), and hexagonal H (sH)[15].

As shown in Figure 1, the sI hydrates comprise two kinds of cages, the small cage (5^{12}) and the large ($5^{12}6^2$). The small cage has is a dodecahedron which has twelve pentagonal faces, and the large cage is a tetrakaidecahedron which has twelve pentagonal faces and two hexagonal faces. The sI hydrate is comprised of 46 water molecules, which forms two 5^{12} cages and six $5^{12}6^2$ cages. Ideally, the small guest gas molecules can occupy both 5^{12} and $5^{12}6^2$ cages, such as methane (CH_4) and carbon dioxide (CO_2); other larger molecules, which forms sI hydrates, cannot enter the small cage due to the large molecular size so that only $5^{12}6^2$ cages can be occupied, e.g. cyclopropane (C-C_3H_6). Therefore, the hydrate number n, which represents the

ratio of the water molecule number and the guest molecule number, is approximately 5.75 for the sI hydrates when the eight cages are fully occupied; and $n \approx 7.67$ for sI hydrates which guest molecule only occupies the large cages.

Figure 2 demonstrates the relationship between the guest molecular sizes and the hydrate cavity ranges[14]. The hydrate number is not fixed due to the driving force effects of hydrate formation, such as temperature and pressure[16].

Similar to the sI hydrates, the sII hydrates are also comprised the small (5^{12}) and the large ($5^{12}6^4$) cages, but the large one is a hexakaidecahedron which has twelve pentagonal faces and four hexagonal faces. The sII hydrate consists of 136 water molecules and forms sixteen 5^{12} cages and eight $5^{12}6^4$ cages. The smallest gas molecules which diameters are less 0.4 nm, such as, nitrogen (N_2) and oxygen (O_2), forms sII hydrates and can occupy all twenty-four cavities ideally with $n \approx 5.67$. Larger guest molecule, e.g. n-butane (n-C_4H_{10}) and CP, will also form sII hydrates but only the large cages are occupied, so the n for this fully occupied sII hydrates is 17. Particularly, the natural gas hydrate is sII hydrate due to the mix of other components, for instance, propane (C_3H_8) and n-C_4H_{10}[12; 14; 17; 18].

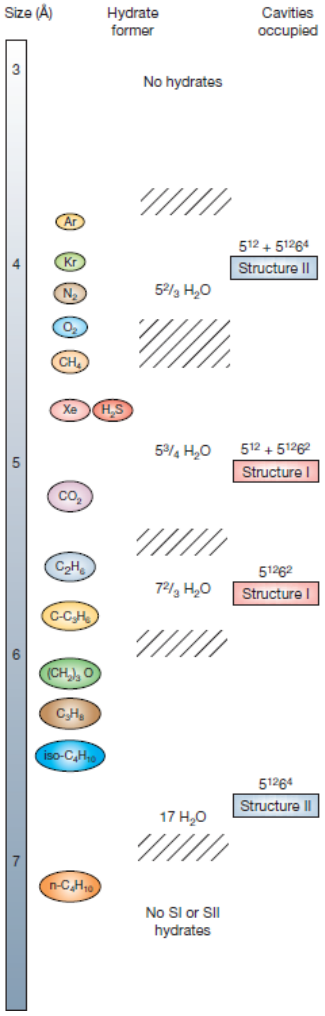

Figure 2 Guest Molecular Sizes and Hydrate Cavity Ranges (cites: Sloan, 2003, Figure 2)

Different form sI and sII hydrates, sH is less common in the natural world. The sH hydrates comprise three kinds of cages, the small cage (5^{12}), another type of small cage ($4^3 5^6 6^3$), and the large ($5^{12}6^8$) cage. The $4^3 5^6 6^3$ small cage has three tetragonal faces, six pentagonal faces, and three hexagonal faces, and the $5^{12}6^8$ large cage has twelve pentagonal faces and eight hexagonal faces. The sH hydrate consists of 34 water molecules. To support the stability of sH hydrates, at least two types of guest molecules, both small and large (0.8-0.9nm) molecules, are required for sH hydrate formation[14; 16]. Thus, the large (0.8-0.9nm) molecules cannot form pure hydrates with water.

2.1.2 Why Studying Methane Hydrate

As methane is the primary component of natural gas, the natures of natural gas are the same as methane to some extent[19]. In addition, considering that the hydrate structure formed by pure methane is sI, which is the simplest structure of clathrate hydrates, methane hydrates are widely researched for both clathrate hydrate study and natural gas study[14; 17]. Some main reasons for studying methane hydrate are presented below.

2.1.2.1 High Gas Capacity

The typical structure of methane hydrate is shown in Figure 3[20]. Due to the cage-like structure (sI) of pure methane hydrate, the capacity of methane contained in hydrate under the standard temperature and pressure conditions could be approximately 150-180 m^3 per cubic meter[7]. The theoretical maximum value is 180 m^3 when all cavities are occupied by methane molecules[21].

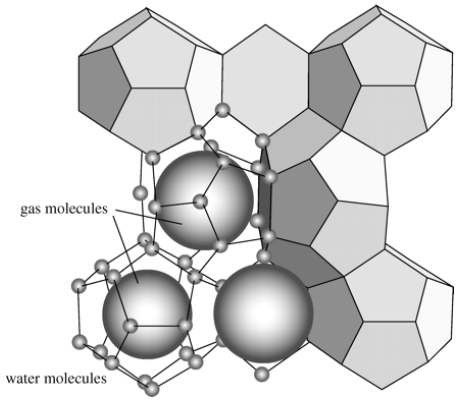

Figure 3 Typical Structure of Pure Methane Hydrate (cites: Maslin et al., 2010, Figure 1)

2.1.2.2 Advantages in Transport and Storage

Currently, natural gas is converted to LNG or CNG for transport or storage purposes to realize the import or export of natural gas resource. Relatively strict transport or storage conditions are required to fulfill the targets. LNG transport and storage should maintain the temperature under -162℃[7]; while CNG is at approximately 0℃ and 18 MPa[14].

These requirements result in the high-cost and high-risk of natural gas transport and storage. Whereas, this issue can be eased by converting gaseous natural gas to solid methane hydrate, which can be transported and stored under the condition approaches to STP (-15℃ and 0.1 MPa)[22; 23].

2.1.2.3 Optimistic Prospect

Recently, the increasing concerns on global environmental issues facilitate the development of the natural gas industry[5]. Compared with other conventional fossil fuel, natural gas emits much less pollution[24], where CO_2, sulfur dioxide (SO_2), nitrogen oxides (NO_x), and $PM_{2.5}$ are considered. International Energy Agency[25] mentioned that natural gas demand will have an optimistic growth rate in the near future compared with other fossil fuels. The estimation is gained based on the tendency of the current global market, energy reserves and energy consumption structure.

2.1.2.4 Broad Distribution and Huge Inventory in Nature

Natural gas is regarded as a kind of fossil fuel, which commonly exists in a gas or solid phase in nature. At present, natural gas is normally mined from natural gas reserves, due to the difficulties of exploiting methane hydrate reserves.

Natural gas reserves are broadly distributed over the world[1] and the proven global is approximately 196.1 trillion m^3 in 2016 (2×10^{14} m^3), where the data is generated from The World Factbook[26]. Relatively, the methane hydrates in nature are normally formed in the deep ocean or beneath permafrost on land. Maslin et al.[20] illustrated the distribution of proven gas hydrate reserves over the world, whereas this kind of natural resource cannot be utilized at present. The estimated volume of methane hydrate dropped by magnitudes from 1990 to 2004[20]. The recent estimates provided by Milkov[27] in 2004 show that the inventory of hydrate-bound gas in the world may be between 1×10^{15} to 5×10^{15} m^3. However, the lower estimated boundary still exceeds the global inventory of natural gas. Thus, methane hydrate in nature is predicted to be a potential alternative energy resource for the future.

2.1.3 Methane Hydrate Formation and Dissociation

2.1.3.1 Methane Hydrate Formation

The visible phenomena are shown in Figure 4, which indicates the process happened during the methane hydrate formation[8]. It is observable that the formation starts from the interface of liquid water and gaseous methane, and the methane formation expands into the bulk water gradually.

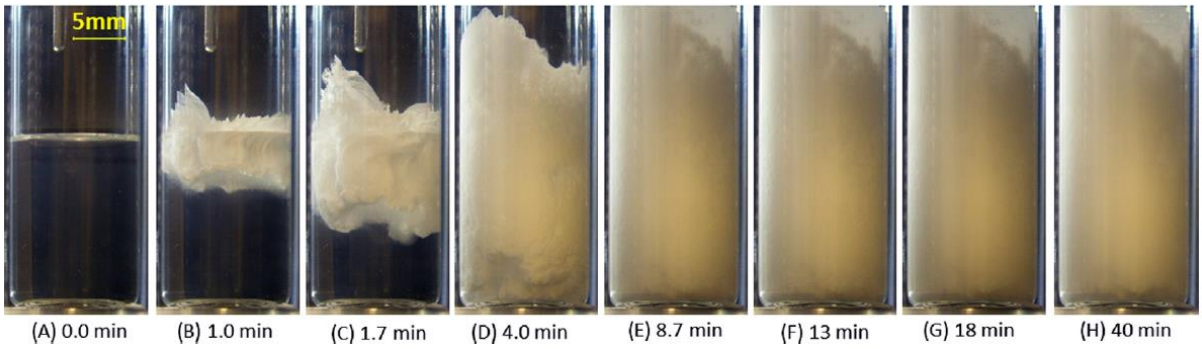

Figure 4 Visible Phenomena of Methane Hydrate Formation (cites: Veluswamy et al., 2016, Figure 1)

When the experiment is conducted, the temperature and pressure data inside the reactor will be collected automatically by the sensors. As shown in Figure 5, the temperature and pressure records are plotted over time[7]. It can be found that an induction time is required for natural gas hydrate formation, which is also called the nucleation period. During this stage, the pressure

decreases slightly; once the nucleation goes to the end, there is a sudden drop in pressure as the methane is consumed for hydration, which is corresponding to Figure 6. The growth period is relatively short compared with the induction time. The formation process is regarded as completed when the pressure does not change obviously for over 2 hours[7].

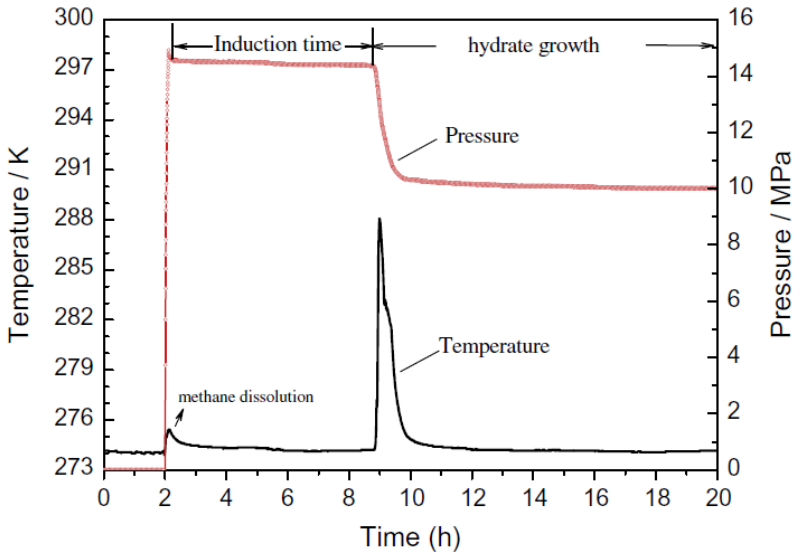

Figure 5 The Curve of Temperature and Pressure Changes vs. Time during the Hydrate Formation (cites: Du et al., 2014, Figure 3)

Figure 6 shows the methane uptake of methane hydrate during the whole formation period[7]. The first stage where the gas uptake increase is not obvious is the nucleation stage. The second stage is the gas uptake goes up rapidly where hydrate starts to form, the slope of the growth period indicates the rate of hydrate formation. In the last stage, the gas uptake is almost constant shows the final uptake of the corresponding test, which represents the capacity of formed

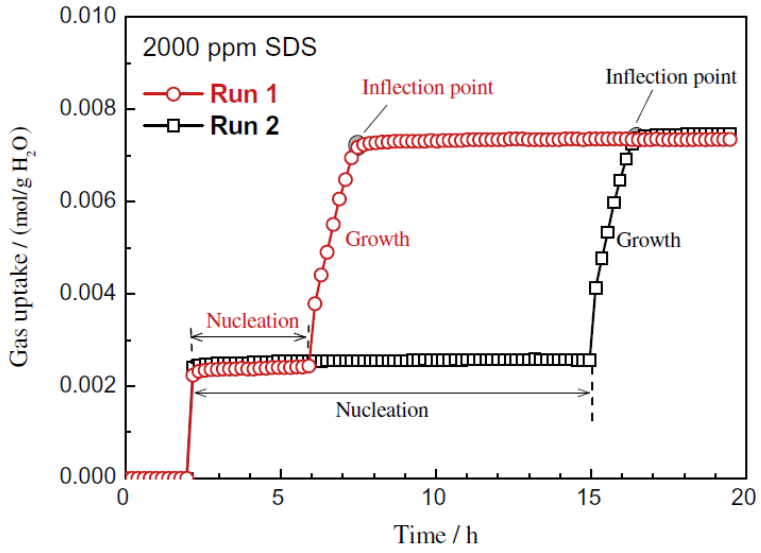

Figure 6 Methane Uptake vs. Time during Methane Hydrate Formation (cites: Du et al., 2014, Figure 4)

methane hydrate. The uptake value may decrease at the end of the whole process in Figure 6, which is due to the hydrate dissociation[7].

2.1.3.1 Methane Hydrate Dissociation

Two kinds of methane hydrate dissociation methods are mentioned in Chong et al. [28]'s article: one is to provide a constant heating temperature; the other is to gradually heat the hydrate. From Chong et al.'s article, Figure 7 illustrates the temperature and pressure profile of the study, where T_{g1} is the gas phase temperature in the experimental vessel which can represent the temperature profile of the experiments. The delays appear in Figure 7 (B) are caused by the endothermic hydrate dissociation process, which indicates the presence of methane hydrate[28].

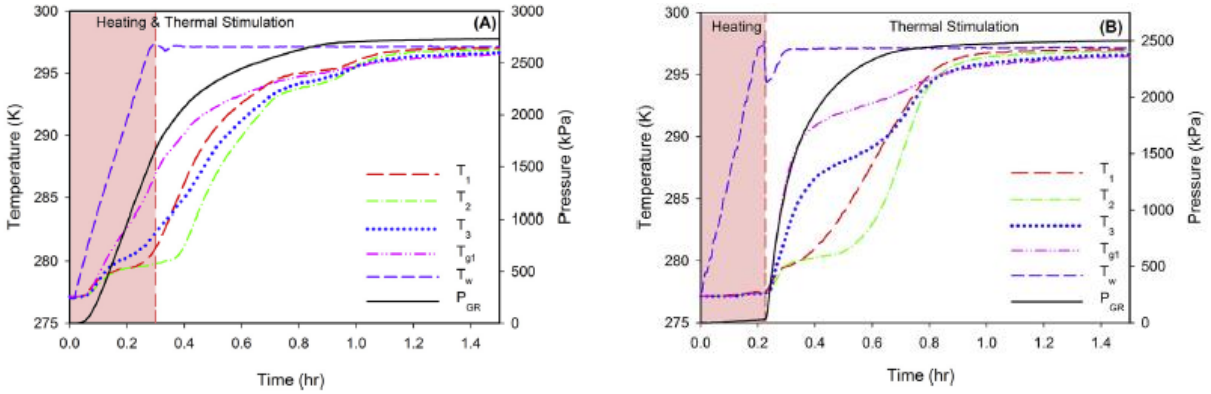

Figure 7 Temperature and Pressure Profiles of (A) Gradual Heating Method; and (B) Constant Heating Method (cites: Chong et al., 2015, Figure 9).

Mimachi et al.[29]'s dissociation experiment places the pre-formed methane hydrate pellets at about -20℃ under the ambient pressure to investigate the storage capability of hydrates. The result shows that the methane hydrate, which is formed at approximately 0℃ and 5.5 MPa in NaCl solution, can be stored for over seven days before dissociation. Therefore, the feasibility of applying SNG for natural gas transport and storage is proved.

2.1.4 Cyclopentane Hydrate Formation and Dissociation

CP hydrate, which has the same hydrate structure (sII) as natural gas, is widely used to mimic natural gas hydrate formation and dissociation process since the CP hydrate can be formed at near ambient temperature and pressure[11; 17; 18]. A temperature profile of CP hydrate formation and dissociation experiment which is conducted by Ho-Van et al.[30] is shown in Figure 8. As CP is water-immiscible liquid, only the temperature needs to be monitored for hydrate study.

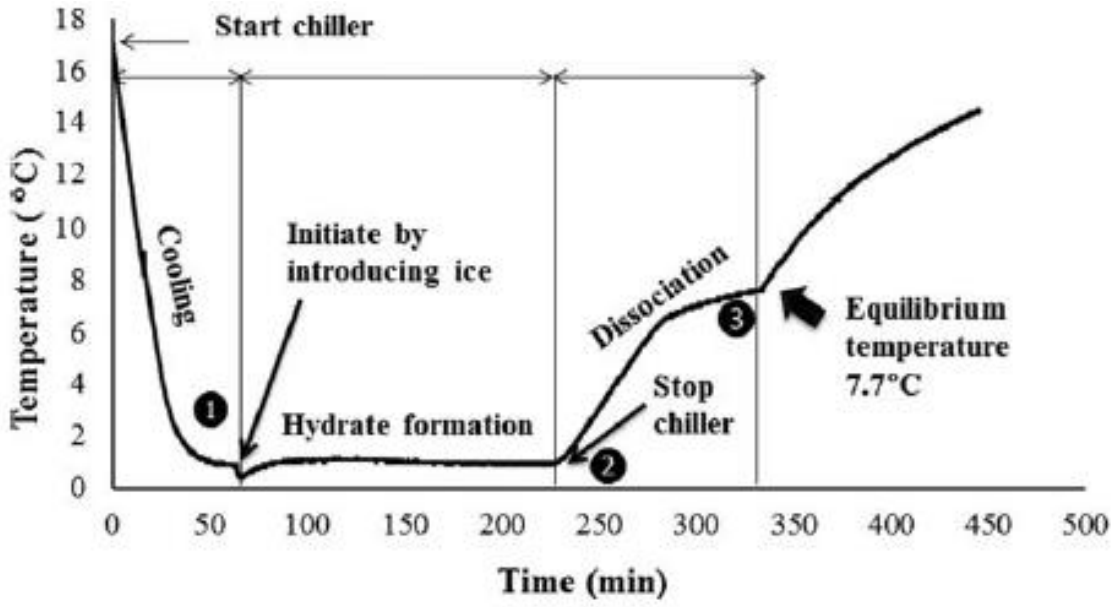

Figure 8 Temperature v.s. Time of CP Hydrate Formation and Dissociation Process in Pure Water (cites: Ho-Van et al., 2018, Figure 2)

As shown in Figure 8 the whole experimental process can be divided into three stages: cooling stage, hydrate formation stage, and hydrate dissociation stage.

2.1.4.1 Cyclopentane Hydrate Formation

In Ho-Van et al.[30; 31]'s experiment, the hydrate formation stage is initiated by injecting ice seed into the system. The introducing of ice seed promotes the hydrate formation progress by shortening the nucleation time[32]. Aman[33] proved that CP hydrate can readily grow based on the provided crystal, either ice crystal or CP hydrates, which significantly reduce the required time for the hydrate formation. The growth process of DI water droplet on the existing CP hydrate particle is recorded by Aman, which demonstrates the microscopic phenomena of hydrate growth at the interface[33].

Nakajima et al.[34] conducted hydrate-forming experiments with CP, water, and surfactant, which are designed for energy storage studies. The phenomena are observed visually from the top of the vessel during hydrate formation (shown in Figure 9 (a-c)). Figure 9 (f) is the hydrate layer attached to the wall of the test vessel.

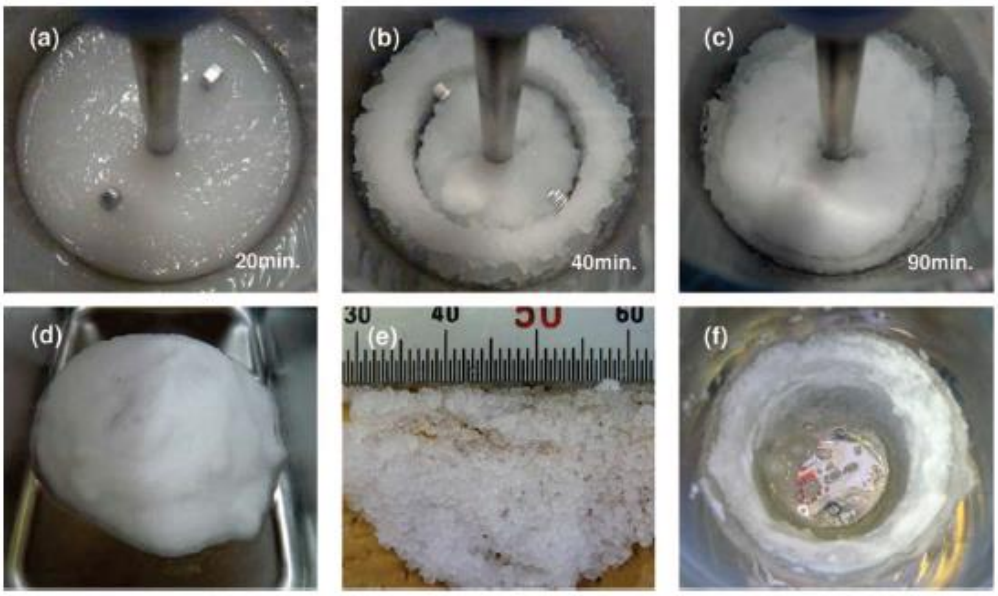

Figure 9 Phenomena of CP Hydrate-Forming Experiments with Surfactant (cites: Nakajima et al., 2008, Figure 5)

2.1.4.2 Cyclopentane Hydrate Dissociation

Similar to methane hydrate dissociation, two types of CP hydrate dissociation procedures are discussed in Ho-Van et al.'s article, that is, the quick procedure and the slow procedure[30]. The main difference between the two procedures is that: the quick procedure "heats" the hydrates with the temperature difference between hydrates and the external environment, so that an integrated temperature profile of hydrate formation and dissociation can be obtained within a few hours; while the slow procedure actually "changes" the hydrate temperature by gradually increasing cryostat temperature 0.1℃ each time until no obvious hydrate particle can be observed in the test tubes.

Both procedures are implemented in Ho-Van et al.'s article so that the phase equilibrium temperatures measured with two procedures are compared. Figure 10 presents the visible phenomena during CP hydrate formation and dissociation experiment which are recorded by Ho-Van et al., and the temperature profiles of experiments applied the quick and slow procedure are demonstrated in Figure 8 and Figure 10, respectively[30].

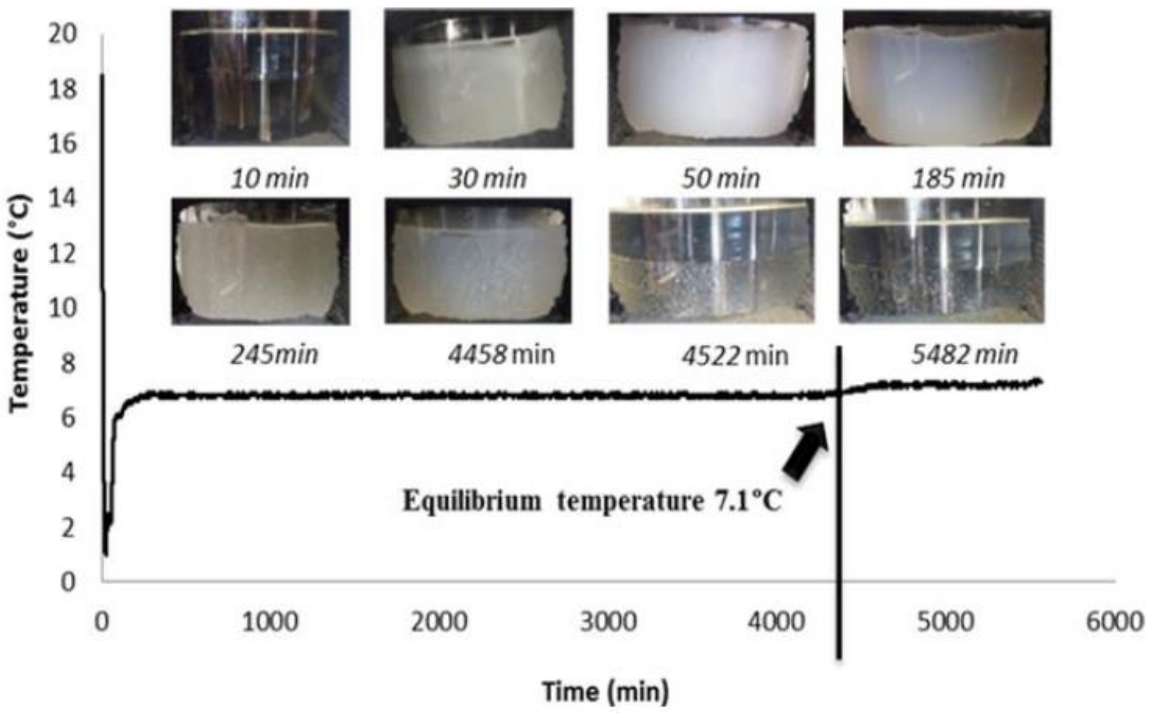

Figure 10 Temperature v.s. Time in Hydrate Dissociation in Pure Water (cites: Ho-Van et al., 2018, Figure 3)

The equilibrium temperature data of CP hydrates in the presence of salts (NaCl, KCl, $CaCl_2$, and NaCl-KCl mix) measured by Ho-Van et al. is illustrated in Figure 11.

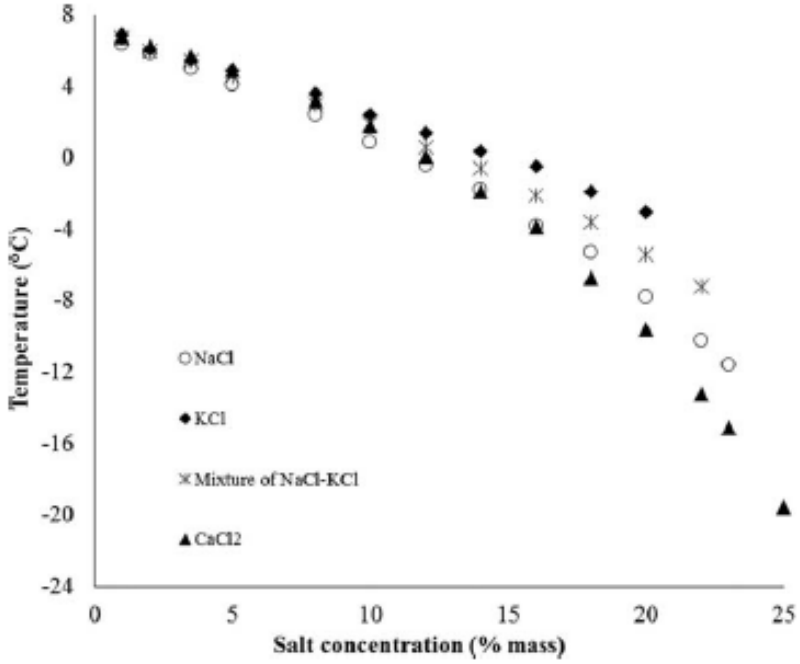

Figure 11 Equilibrium Temperature v.s. Salt Concentration in Presence of Salts (cites: Ho-Van et al., 2018, Figure 4)

2.2 Hydrate Formation Inhibition and Promotion

Hydrate formation can be affected by many reasons, for example, the change of temperature or pressure, with/without stirring[7; 9], additives[7; 9; 35-39], etc.

2.2.1 Driving Force

The primary driving forces for hydrate formation are provided by the difference between system and phase equilibrium temperature and pressure. Particularly, for liquid guest molecules, subcooling is the key driving force since the system pressure does not have significant effects on the liquid phase reaction.

Mali et al. [40] investigated the effect of subcooling on hydrate formation with the natural gas and water system. The tests verified that the induction time for hydrate formation is stochastic. But, their further study on data processing discovered the relationship between the distribution of induction time and subcooling. That is, the induction time of hydrate formation is generally reduced with the increasing of subcooling to some extent.

It is also found that the induction time is increased due to the increase of pressure at a constant subcooling level[40]. The discovered results consistent with Arjmandi et al.[41]'s conclusions that the increasing system pressure has a negative impact on hydrate formation.

2.2.2 Mechanical Method

Stirring is a kind of mechanical methods to break the thin cyclopentane hydrate film at the interface of cyclopentane and brine so that the liquid-liquid surface of two phases can be greatly improved to reduce the hydrate nucleation time[7; 42]. Du et al. have proved that agitation/stirring can significantly increase the hydrate formation rate than that under the static state[9].

2.2.3 Additives

The inhibitors of the hydrate formation process include salts, alcohol[43], and L-proline[44] which works as the hydrate formation as a thermodynamic hydrate inhibitor (THI).

Mostly, the amino acids can enhance the kinetics of methane hydrate formation as an anionic surfactant, Bhattacharjee et al.[45] and Veluswamy et al.[46] have proved and tested the effects of three types of common amino acids, that is, L-histidine[45; 46], L-tryptophan[46], and L-arginine[46].

Sulfonated lignin (SL)[47] is also a novel anionic surfactant for promoting hydrate formation. Mofrad et al.'s[47] experiments show that the final uptake of formed methane hydrate with of

SL and Sodium Dodecyl Sulfate (SDS) at same concentration are similar; while the growth rate of SL is slower than SDS and it requires a higher pressure in the reactor.

Recent studies have investigated sets of surfactants that have similar structures. For example, Du et al.[7] have compared the effects of promoters which have 12-C but with different functional groups; and Su et al.[37] have investigated the thermodynamic effect on methane hydrate formation with a set of organic salts which have the same cation and anion but different carbon chain length.

In addition to surfactants, other substances, such as graphene and its derivatives[48-50], nanoparticles (iron(II,III) oxide (Fe_3O_4)[36; 51] and cupric oxide (CuO)[35]) with a surfactant to suspend in water, have also been investigated.

2.3 Water Activity

2.3.1 Introduction of Water Activity

A definition has been given to the water activity (a_w), that is, 'it is a measure of how easy the water content may be utilized'[52]. In other words, the water activity can also be interpreted as the capability of water to hydrate with other materials. The capability increases with the value of a_w from zero to one, where, $a_w = 0$ indicates that no water is available for hydration, whereas the other extreme is that all water is available, namely $a_w = 1$.

2.3.2 Factors of Affecting Water Activity

The water activity can be affected by adding solutes or changing circumstance conditions (temperature and pressure)[52; 53], where the water structure can be changed. With the empirical equations, the water activity of a specific situation can be estimated with another known condition. However, there are strict limitations when applying an empirical equation since mostly these equations only suitable for some states. Chaplin[52] stated the existence of salts will reduce the water activity, and theoretically, the water activity decreases proportionally with the increase of salt molality in an ideal situation. Also, he pointed out the water activity may ideally rise with the increase of temperature and pressure, but some exceptions exist.

2.3.3 Effects of Additives on Water Activity

Sowa et al.[54] studied the effects of strong monovalent salts on hydrate formation at high and low concentration respectively. The experiments found these monovalent salts will inhibit the methane hydrate formation at high concentration (>1 M), but some salts except NaCl promoted the formation at low concentration. This research corresponds to a similar study reported by Farhang et al.[55], which discovered the influence of sodium halide ions on CO_2 hydrate

formation. An assumption was constructed based on the experimental results. The hydrate formation should be substantially influenced by changing the water activity[54; 56]. This opinion can be supported by Wang et al.'s[57] research. The influences of different anions and cations on the kinetics of water were studied with Nuclear Magnetic Resonance method (NMR method). Experimental data indicated the impacts of ions on water structure. The water activity decreases when "kosmotropic" ions, such as SO_4^{2-} and CH_3COO^-, which contribute to the association between water molecules; in contrast, a_w will increase when "chaotropic" ions, such as Br^- and NO_3^-.

2.3.4 Effects of Electric and Magnetic Field on Water Activity

Chaplin[52] concluded the effects of the electric and magnetic field on water structure. His researches support that the electric field can accelerate the ice formation process by weakening the hydrogen bonds under low field strength; while the acceleration is proceeded by damaging the hydrogen bonds completely when the field strength is very high. The mechanism is explained microscopically. Also, the Raman spectra show the distances between O-H (hydrogen bonds) were increase, the sizes of water clusters were reduced[58]. However, other substances, such as O_2^- and H_2O_2, may be introduced to the system[59].

Conversely, the effects of the static magnetic field on water structure will promote the hydrogen-bonding by increasing the order of water molecules[52; 60]. Firoozabadi et al.[51] conducted an investigation on the relation between water structure and electrolyte concentration under in magnetic field[61]. The experimental results show that the exiting of the magnetic field has a negative impact on water activity when NaCl electrolyte solutions at low concentration (1 M) or no concentration (0 M). The number of hydrogen bonds and the ability of hydrogen bonding increase with the strength of the magnetic field. The structure of hydrogen bonds is dominated by the properties of water molecules. Instead, NaCl solution at high concentration (5 M) has a positive influence on water activity. The water activity is enhanced as hydrogen bonds is reduced and weaker in this condition. This is due to the damage of hydrogen-bonding structure which is caused by the mobilities of the intensive ions under the magnetic field[61]. However, Shu et al.[38] conducted sets of experiments to figure out the effects of static/rotating magnetic field on HCFC-14b gas with different poles and strength, which have an inconsistent conclusion on static condition.

In Chaplin's[52] study, a compound field is mentioned when electric and magnetic fields exist at the same time. This kind of field may lead to complex results since the single electric field and a single magnetic field will have opposite effects on the pure water structure.

The water activity change caused by electric/magnetic/electromagnetic field can be maintained for a period of days[59; 62]

2.4 Hu-Lee-Sum Correlation

Hu et al.[18; 63; 64] proposed a new correlation for predicting the hydrate suppression temperature which in consideration of the types of salt and their concentrations.

The Hu-Lee-Sum correlation is expressed the hydrate depression temperature as a polynomial equation of effective mole fraction (X)[18]. The correlation is presented as Equation 1.

$$\frac{\Delta T}{T_0 T} = -\frac{nR}{\Delta H_{diss}} \times \ln a_w = C_1 X + C_2 X^2 + C_3 X^3$$

Equation 1 Hu-Lee-Sum Correlation

where, ΔT is the hydrate depression temperature, $\Delta T = T_0 - T$, K; T_0 is the hydrate dissociation temperature with fresh water, K; T is the hydrate dissociation temperature with the electrolyte, K; n is the hydration number which is obtained from $\text{Guest Molecule} + \text{nH}_2\text{O} = \text{Guest Molecule} \cdot \text{nH}_2\text{O}$, the value of n reaches the minimal value when the hydrate is fully occupied; ΔH_{diss} is the hydrate dissociation enthalpy, J; R is the molar gas constant, R=8.314 $\text{J}/(\text{mol} \cdot \text{K})$; a_w is the water activity; C_1, C_2, and C_3 are fitted coefficients; and X is the effective mole fraction, which can be calculated with equation below (shown as Equation 2[18]).

$$X = \sum_{j=salts} \sum_{i=ions} |z_{j,i}| x_{j,i}$$

Equation 2 Effective Mole Fraction Calculation

where, i and j represent the ion and the salt, respectively; z is the charge number; and x is the mole fraction of the ion.

In Hu et al.'s articles, the $nR/\Delta H_{diss}$ is considered as a constant when the guest molecule composition and dissociation enthalpy are known. The simplified Hu-Lee-Sum correlation is shown as Equation 3[18; 63; 64].

$$\frac{\Delta T}{T_0 T} = \beta \times \ln a_w = C_1 X + C_2 X^2 + C_3 X^3$$

Equation 3 Simplified Hu-Lee-Sum Correlation

where, β is the constant ($\beta = -nR/\Delta H_{diss}$), which only depends on the hydrate component and composition.

The Hu-Lee-Sum correlation can be used for predicting the hydrate suppression temperature which can be applied to both sI and sII hydrates. Moreover, the water activity can be estimated with the known constants and effective mole fraction.

2.5 Knowledge Gap in Current Literature

The literature review in this Chapter covers the understandings and information about methane hydrate and its formation process. A large amount of work has been done on methane hydrate studying, but limited researches are carried out on natural gas hydrate study which may due to the uncertainty of natural gas components and compositions. Therefore, as mentioned in the previous section, CP is selected to mimic natural gas hydrate formation and dissociation.

Despite the phase equilibrium temperature of CP hydrates were studied by others[30; 31], the available data for researching are still limited. Particularly, equilibrium temperature data for high-valence salts, such as $AlCl_3$, are missing. The lack of reliable equilibrium data results in barriers for other studies, e.g. equilibrium temperature data are required for controlling the subcooling (variable).

2.6 Research Proposals and Hypotheses

2.6.1 Proposals

The research proposals for this thesis include:

1) Measure the freezing points of three types of electrolytes;
2) Observe the phenomena of CP hydrate formation and dissociation process;
3) Measure the phase equilibrium temperature data of CP hydrates formed in three types of electrolytes;
4) Analyse the relationships between the equilibrium temperature and concentrations.

2.6.2 Hypotheses

The corresponding hypotheses are listed:

- The measured freezing points of NaCl and $CaCl_2$ should be close to the estimated data; possible linear correlations between freezing points and salt molality.
- CP hydrate formation should start at the interface of CP and solution; the CP hydrate growth and ice-like CP hydrate particles should be able to observe; the equilibrium temperature of CP hydrate could be monitored.

- The measured equilibrium temperature should decrease with the increase of salt mass fraction; the effectiveness of salt solution may be NaCl > $CaCl_2$ > $AlCl_3$ based on the literature.
- Possible thrice polynomial relationships exist between $\Delta T/T_0 T$ and the effective mole fraction considering Hu-Lee-Sum correlation; the relationship between water activity and effective mole fraction may be discovered.

Chapter 3: Experimental Apparatus and Methodology

3.1 Experimental Apparatus

3.1.1 Scheme

The simplified experimental scheme for the experiment is shown in Figure 12.

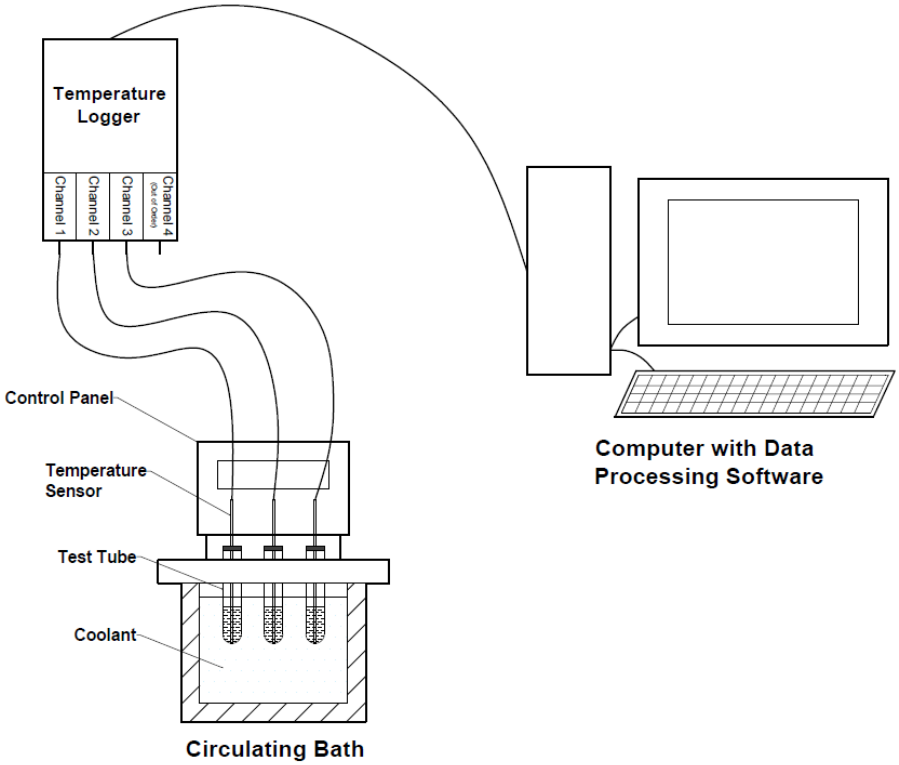

Figure 12 Simplified Schematic Diagram for Experimental Apparatus

3.1.2 Cryostat

The cryostat is a device that can maintain the sample at low temperature. *Thermo Scientific NESLAB RTE-7 Circulating Bath* is applied as cryostat for this experiment, which is shown in Figure 13. The bath is filled with coolant instead of water since the bath temperature which below the water freezing point (0℃) is required. Some key parameters of the bath are listed in Table 1[65].

Table 1 Specifications of Circulating Bath

Temperature Range	-25℃ to 150℃
Stability	±0.01℃
Bath Volume	7 L
Dimensions (H×W×D)	60.01cm×23.5cm×44.5cm

Figure 13 NESLAB RTE-7 Circulating Bath

3.1.3 Temperature Logger

A 4-channel real-time differential (RTD) data acquisition module OMEGA® PT-104A[66] (shown in Figure 14) is applied in the experiment for monitoring the temperature during cyclopentane hydrate formation and dissociation processes, which has both high accuracy at approximately 0.01℃ and high resolution at around 0.001℃[67]. As four channels are available, multiple tests under the same conditions can be conducted simultaneously.

Figure 14 OMEGA® PT-104A

3.2 Experimental Materials

3.2.1 Cyclopentane (C_5H_{10})

98 wt% pure CP (purchased from Sigma-Aldrich) is selected for the experiment. Its molecular structure is shown in Figure 15, and key specifications are generated in Table 2.

Table 2 Key Specifications of CP (Refers to Chemwatch SDS[68])

Formula	C_5H_{10}
Molecular Weight	70.13 g/mol
Reagent Grade	98%
Relative Density (Water = 1)	0.75
Relative Density (Air = 1)	2.42
Odor	Petroleum-like odor
Solubility	Insoluble in water
Chemical Stability	Stable
Hazards	Flammable liquid

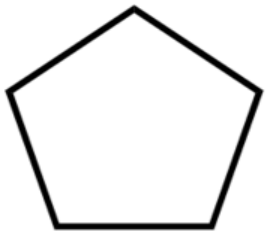

Figure 15 Molecular Structure

The CP hydrate structure is sII, which is the same as natural gas hydrate structure[12; 17; 69]. It can be studied as a model system for understanding natural gas hydrate, as CP hydrate can be formed at a near ambient pressure and temperature[11]. Especially, CP hydrate with deionized water (DI) may form at approximately ice point, which equilibrium temperature is 7.7℃[17].

3.2.2 Brine

For this project, the concentration of the brine is prepared in molality to reduce the complexity of the preparation process, so that the solution densities do not need to be considered. Three types of chloride solutions are studied: NaCl, $CaCl_2$, and $AlCl_3$ solutions. All reagents are purchased from Sigma-Aldrich. The specifications of the three salts are listed in Table 3.

Table 3 Specifications of Chloride Salts (Refers to Chemwatch SDS[70-72])

Chlorides Types	Sodium Chloride	Calcium Chloride	Aluminium Chloride
Purity (wt%)	≥99.5	≥97	99
Molecular Weight (g/mol)	58.44	110.99	133.3
pH as a solution (1%)	6.7-7.3	N/A	3.2
Chemical Stability	Stable	Stable	React with alkaline
Solubility in Water	Miscible	Miscible	Miscible/React
Hazards	N/A	N/A	Corrosive

3.2.3 Coolant

Nulon Green Premium Long Life Coolant 100% Concentrate[73; 74] is used for cooling samples temperature down below the ice point since the water cannot satisfy the requirement as an intermediate. The selected concentrated coolant is suitable for an experimental temperature range from -37℃ to 128℃ when it is mixed with water at the ratio of 1:1. In this project, due to the temperature range of circulating bath mentioned above, the lowest experimental temperature which is detectable should not lower than -15℃. Therefore, the selected coolant meets the experiment requirement. The *Nulon* coolant selected is shown in Figure 16.

Figure 16 Nulon Coolant

3.2.4 Alcoholic Hydroxide Solutions

Alcoholic hydroxide solutions are required for the cleaning of glassware to avoid the contamination from previous experiments. Alcoholic hydroxide is prepared with potassium hydroxide (KOH), ethanol (C_2H_5OH) and DI water. The volumetric ratio of water to ethanol is 1:8. Procedure for solution preparation includes[75; 76]:

- Adding 30g KOH into 100ml DI water, stirring until dissolved;
- Add the KOH solution to 800ml ethanol in a plastic container;
- Stir to mix KOH solution and ethanol completely.

3.3 Experiments Preparation

3.3.1 Glassware Cleaning

The glassware needs to be cleaned with the prepared alcoholic hydroxide solutions by soaking into the solutions and maintains for at least 30min. After taking out from the solutions, the glassware is washed with tap water for over seven times and with DI water for three times in additionally. Therefore, the effects of contaminations and ions can be eliminated.

3.3.2 Brine Preparation

The fresh brine is prepared with salt and DI water. The analytical balance is used for weighting salts and water, which has a high resolution of 0.001g.

The definition equation of molality (b) is shown as below:

$$b = \frac{n_{\text{salt}}}{m_{\text{water}}}$$

Equation 4 Definition Equation of Molality

where n_{salt} is the mole of the salt used for solution preparation, mol; m_{water} is the mass of the solvent which is water, g.

The effective mole fraction (X) of the brine can be obtained with the Equation 2 mentioned in Section 2.4, detailed calculations refers to APPENDIX-D. As the brine are prepared on the molality base, the equivalent mass concentration (ω) of brine can be calculated with the following equation:

$$\omega = \frac{n_{\text{salt}} \times \text{MW}_{salt}}{(n_{\text{salt}} \times \text{MW}_{salt} + m_{\text{water}})} \times 100\%$$

Equation 5 Equivalent Mass Concentration (ω)

where MW_{salt} is the molecular weight of the salt, g/mol. Thus, the conversion relationship between molality and mass fraction can be presented with Equation 6 and Equation 7.

$$\omega = \frac{b \times \text{MW}_{salt}}{(b \times \text{MW}_{salt} + 1000)} \times 100\%$$

Equation 6 Conversion Relationship from Molality to Mass Fraction

$$b = \frac{1000\ \omega}{(100 - \omega)/\text{MW}_{salt}}$$

Equation 7 Conversion Relationship from Mass Fraction to Molality

The concentrations of prepared brine for hydrate formation are listed in Table 4. Detailed calculations of each solution can be found in APPENDIX-E. The concentrations of brine prepared for the experiments do not exceed its saturation state.

Table 4 Details of Prepared Brine

Solution No.	Solvent	NaCl (mole/kg H_2O)	$CaCl_2$ (mole/kg H_2O)	$AlCl_3$ (mole/kg H_2O)	Effective Mole Fraction	Equivalent Mass Fraction (wt%)
1	DI water	-	-	-	0.0000	0.00
2	DI water	0.5	-	-	0.0177	2.84
3	DI water	0.7	-	-	0.0246	3.93
4	DI water	1.0	-	-	0.0347	5.52
5	DI water	1.5	-	-	0.0512	8.06
6	DI water	2.0	-	-	0.0672	10.46
7	DI water	-	0.2	-	0.0142	2.17
8	DI water	-	0.5	-	0.0351	5.26
9	DI water	-	0.7	-	0.0486	7.21
10	DI water	-	1.0	-	0.0683	9.99
11	DI water	-	1.5	-	0.0999	14.27
12	DI water	-	-	0.1	0.0107	1.32
13	DI water	-	-	0.2	0.0213	2.60
14	DI water	-	-	0.35	0.0369	4.46
15	DI water	-	-	0.5	0.0521	6.25
16	DI water	-	-	0.7	0.0720	8.53
17	DI water	-	-	1.2	0.1193	13.79

Additionally, more NaCl solutions with different concentrations are prepared for experiment startup, which the correlation of NaCl solution equilibrium temperature and its concentration can be obtained with the same experimental apparatus. Table 5 lists the solutions with a variety of concentration for the pre-experiments.

Table 5 NaCl Solutions for Pre-experiments

Molality (mole/kg H_2O)	0.5	0.6	0.7	0.8	1.0	1.5	2.0	3.0	4.0
Equivalent Mass Fraction (wt%)	2.84	3.39	3.93	4.47	5.52	8.06	10.46	14.92	18.95

3.4 Experimental Process

3.4.1 Experimental Setup

The experimental setup for CP hydrate formation and dissociation experiments is shown in Figure 12 (Section 3.3.1). The hydrate formation happens in the test tubes which are put in the circulating bath. The bath is filled with coolant (Figure 17 (a)) for cooling down the samples to the desired temperature. The sensors of temperature logger are put in the test tubes (Figure 17 (b)), which are placed in the solution phase and reach the bottom, to monitor the temperature of the experiment. The monitored data are transferred through temperature logger to the computer (Figure 17(c)) and stored for further processing.

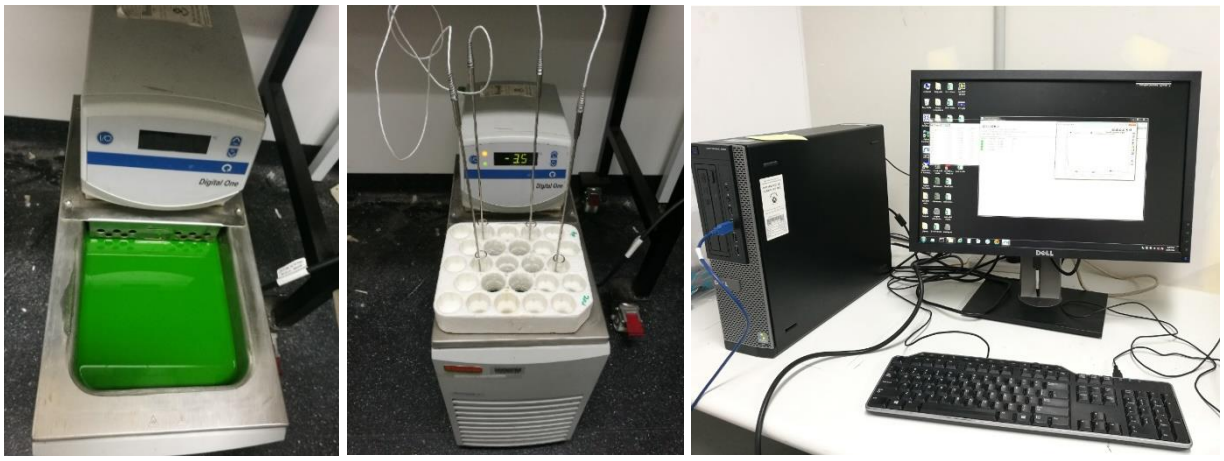

(a.) (b). (c).

Figure 17 Experimental Setup

3.4.2 Calibration for Temperature Logger

Before the tests, the calibration for temperature logger is required to increase the reliability of experimental data. This purpose is achieved by carrying out the experiment to measure the freezing point of DI water, which should be 0℃ theoretically, at the ambient temperature and pressure.

In addition, another handy thermometer is also used as a reference, which is shown in Figure 18. This data logging thermometer has a lower resolution of 0.01℃ and a lower accuracy of ±025℃[77]. It can be regarded as a reference because it is a relatively new product so that its displayed temperature is close enough to the real ambient temperature.

Figure 18 Thermometer Used as a Reference

The procedures for calibration include:

- Set bath temperature 5℃ lower than the ice point of DI water;
- Add 5mL DI water into three test tubes and put temperature probes in each tube;
- Place the tubes in the circulating bath and start logging the temperature;
- Stir after the tubes are entirely supercooled to freeze;
- Process the data to figure out the recorded freezing point;
- Compare with the theoretical freezing point, and the difference values are the deviations of the temperature logger.

3.4.3 Preliminary Experiments for Salt Solution Freezing Point

Preliminary experiments for salt solution freezing point are designed to avoid the extreme conditions during the hydrate formation process, that is, the salt solutions freeze before CP hydrates form.

The procedures for freezing point tests are similar to the calibration test:

- Set bath temperature 5-10℃ lower than the estimated salt solution freezing point;
- Add 5mL salt solution into the test tubes and put in the temperature probes;
- Place tubes in the bath and start logging the temperature;
- Stir after the tubes are entirely supercooled to freeze;
- Process the data to figure out the recorded brine freezing points;
- Consider the deviation of temperature logger and obtain the exact freezing points.

The estimated freezing points of NaCl and $CaCl_2$ can be obtained from the literature, while the detailed information of $AlCl_3$ solutions is limited. APPENDIX-C shows the relationship between NaCl freezing point and its molality[78]. Based on the graph (Figure 37), the estimated freezing points of NaCl solutions are listed in Table 6.

Table 6 Estimated Freezing Points of NaCl

Molality (mol/kg H_2O)	Estimated Freezing Point (℃)
0	0
0.5	-1.702
0.6	-2.027
0.7	-2.367
0.8	-2.714
1.0	-3.386
1.5	-5.126
2	-6.937
3	-10.798
4	-15.161

Similarly, the estimated freezing points of $CaCl_2$ can also be gained with the relationship between $CaCl_2$ freezing point and its molality[78; 79]attached in APPENDIX-C Figure 38. The estimated results of $CaCl_2$ is listed in Table 7.

Table 7 Estimated Freezing Points of $CaCl_2$

Molality (mol/kg H_2O)	Estimated Freezing Point (℃)
0	0
0.2	-1.036
0.5	-2.643
0.7	-3.775
1.0	-5.693
1.5	-9.723

3.4.4 Preliminary Experiments for Accelerating Hydrate Formation

Even the CP hydrates can be formed under the near ambient conditions[11], it will still take a long, stochastic time for induction under static state[80; 81]. Therefore, to accelerate the hydrate formation progress and reduce the time required for nucleation, some approachable methods are considered in these experiments.

3.4.4.1 Intermittent Stirring Provided

In this experiment, the cyclopentane and brine are stirred manually to increase the heat transfer and improve the mass transfer at the interface. The stirring is compulsory for this project, otherwise, days are required for hydrate nucleation. As the intermittent agitation is provided manually, the hydrate formation rate can be promoted to some extent. However, this mechanical method will also introduce disturbances which may lead to temperature fluctuations and be recorded by the logger.

3.4.4.2 The ratio of CP and Solution Selected

The tests with different ratios of CP and solution are prepared for the preliminary experiments. Theoretically, the stoichiometric ratio of CP and water should be 1:17 (Equation 8), since the CP hydrates are sII hydrate[17]. Consider the molecular weight of CP and water, the volumetric ratio of CP hydrate is calculated to be CP: water = 1:3.

$$C_5H_{10} + 17H_2O = C_5H_{10} \cdot 17H_2O$$

Equation 8 Stoichiometry of CP Hydrate

Thus, the volumetric ratios selected for the preliminary ratio test including 1:3, 1:1, 2:1 and 3:1, since excess CP is required to reduce the time for nucleation and avoid the effects of volatilization. These tests are evaluated visually to select a suitable ratio for the experiment.

For this hydrate formation experiment, ratio 2:1 is chosen due to its better performance which will be discussed later.

3.4.4.3 Subcooling Decided

Subcooling is the key driving force of this experiment. As mentioned in Section 2.2.1, the hydrate formation rate can be increased with increasing subcooling. Therefore, to maximize the driving force of this project, the experimental temperatures are decided to be set just above the brine freezing points. The freezing points are obtained from the preliminary experiments described in Section 3.4.3.

3.4.5 Cyclopentane Hydrate Formation

The preliminary experiments are necessary for proving the reliability of the designed experiments. Also, these tests provide essential information for CP hydrate formation.

After completing the preliminary experiments, the CP hydrate formation experiment is conducted at the ambient temperature and pressure. Key procedures for hydrate formation are listed below:

- Set circulating bath temperature above the measured brine freezing point, and wait for over 10min before the test to ensure bath temperature reaches the stability;
- Rinse the test tube with the salt solution twice;
- Add 2mL brine and 4mL CP in each test tube (volumetric ratio of CP and brine = 2:1);
- Put the temperature probes into the tubes and reach the bottom;
- Place the test tubes in the circulating bath and start logging the temperature;
- Start stirring after 20min;
- Intermittent agitation is provided manually at a nearly constant speed;
- Observe the hydrate formation process visually during the experiments.

The CP hydrate formation process completes when a significate amount of hydrate appears.

3.4.6 Cyclopentane Hydrate Dissociation

The CP hydrate dissociation experiment can be conducted once a sufficient amount of hydrate formed in the test tubes. Two types of hydrate dissociation methods are designed for this experiment: the quick dissociation process and a slower dissociation process[31; 82].

3.4.6.1 The Quick Hydrate Dissociation Process

The quick dissociation process requires much less time for hydrate dissociation by simply put cyclopentane hydrate at the room temperature. The heat is transferred directly between hydrate and atmosphere so that the dissociation is enhanced by a large temperature difference.

For this project, the quick dissociation process is selected to measure the possible phase equilibrium temperature of CP hydrates. The key procedures for the quick hydrate dissociation are listed as following:

- Take the test tubes out of the circulating bath;
- Place the test tube in a conical flask and put the flask at the surface of coolant, so that the heat transfer between CP hydrates and external environment can be reduced to slow down the dissociation process;
- Remove the excess CP from the test tubes before dissociation;
- Stir during the dissociation process to ensure the homogeneous detected temperature;
- Collect the data with temperature logger;
- Observe the dissociation process visually during the experiments.

The CP hydrate dissociation process completes when no hydrate can be observed in the test tube by eyes. Note down the temperature when all hydrates disappear.

3.4.6.2 The Slower Hydrate Dissociation Process

Compared with the quick dissociation, the slower dissociation process is conducted within the cryostat instead of taking out of the bath. This method takes rather a long period for each test. For the slower dissociation process, the bath temperature is controlled manually and gradually increased by 0.1℃ each time. Hours or days are required for observation after changing the set temperature. If a large amount of hydrates still exists in the test tube, then repeat increasing the set-point and observe for another long period. The procedures are repeated until almost all hydrates disappear after one iteration. The set temperature at the final stage can be regarded as the phase equilibrium temperature.

3.5 Data Progressing

With OMEGA® PT-104A, the temperature data of the experiment are detected with the temperature probes and transferred through temperature logger to the computer. The data are received and initially progressed with the corresponding OMEGA® software automatically, which can provide direct monitoring of hydrate formation and dissociation process through the real-time data spreadsheet and curves.

For further studies and discussions, the stored data are copied from the OMEGA® software and progressed with MS Excel and Origin software to obtain the accurately measured equilibrium temperature and discover the relationships of CP hydrate phase equilibrium temperatures and brine concentrations.

Chapter 4: Result Analyses and Discussions

4.1 Temperature Logger Calibration

The deviations of temperature logger are calibrated with DI water follows the procedures listed in Section 3.4.2. The temperatures detected by three channels of logger are recorded and plotted in Figure 19.

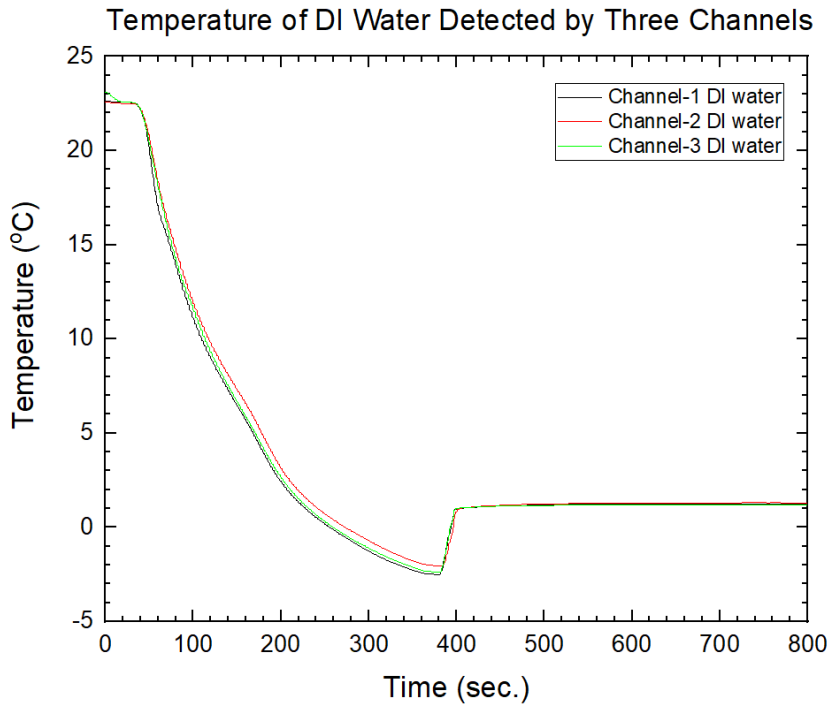

Figure 19 Temperature of DI Water Freezing Point Test (Detected by Three Channels)

As shown in the figure, the DI water was supercooled below the theoretical ice point (0°C). The supercooling condition is compulsory since the crystallization of the water happens during this period. The supercooled liquid is metastable so that the congealment of DI water could start by seeding crystals or introducing agitations.

Figure 19 demonstrates that the supercooled DI water starts converting to solid ice at approximately 400 seconds due to the stirring. The monitored temperature presents a sudden increase and backs to the liquid freezing point directly. The measured DI water freezing points of three channels are shown in Table 8.

Table 8 Measured Freezing Point of DI Water (Detected with Three Channels)

	Channel-1 (Ch-1)	Channel-2 (Ch-2)	Channel-3 (Ch-3)
Theoretical Freezing Point (°C)	0	0	0
Measured Freezing Point (°C)	1.00	1.03	1.02
Deviation of Temperature Logger, T_M-T_{Theo} (°C)	1.00	1.03	1.02

Additionally, the real temperature of the bath is measured with the sensor. The monitored results show that the real bath temperature is generally 2.2℃ higher than the set-point displayed on the screen. This deviation of bath temperature needs to be considered when setting the cryostat target temperature.

4.2 Measured Freezing Point of Salt Solutions

The freezing points of three types of brine (NaCl, $CaCl_2$, and $AlCl_3$) in different concentrations are discussed in this section.

4.2.1 Prepared NaCl Solution Freezing Points

The NaCl solutions are prepared based on the designed concentrations listed in Section 3.3.2 and Section 3.4.3. Table 9 lists the real molality of prepared NaCl solutions and their equivalent mass fractions; also, the estimated NaCl freezing points, the measured results and the deviations are presented. The estimated freezing points, which are gained based on Liu et al.[78]'s data, and the measured NaCl freezing points are plotted in Figure 20.

Table 9 Freezing Points of Prepared NaCl Solutions

Molality of Prepared Solution (mol/kg H2O)	Equivalent Mass Fraction (%)	Estimated Freezing Point (℃)	Measured Freezing Point (℃)	Deviation T_M-T_E (℃)
0	0	0	0	0
0.50	2.84	-1.702	-1.728	-0.026
0.60	3.39	-2.027	-2.089	-0.062
0.70	3.93	-2.367	-2.462	-0.095
0.80	4.47	-2.714	-2.627	0.087
1.00	5.52	-3.386	-3.781	-0.395
1.50	8.06	-5.126	-5.324	-0.198
2.00	10.46	-6.937	-6.883	0.054
3.00	14.92	-10.798	-*	-
4.00	18.95	-15.161	-*	-
* Circulating bath temperature range cannot fulfil the subcooling requirement of freezing.				

Figure 20 (a.) shows the freezing point of NaCl solution over mass fraction; while in Figure 20 (b.), the freezing point is plotted over molality. Additionally, linear fitting analysis is conducted and exhibited in Figure 20 (b.). The slopes of the linear fits of estimated and measured data are approximately -3.79 and -3.49, respectively. The corresponding R^2 are 0.9971 and 0.9963.

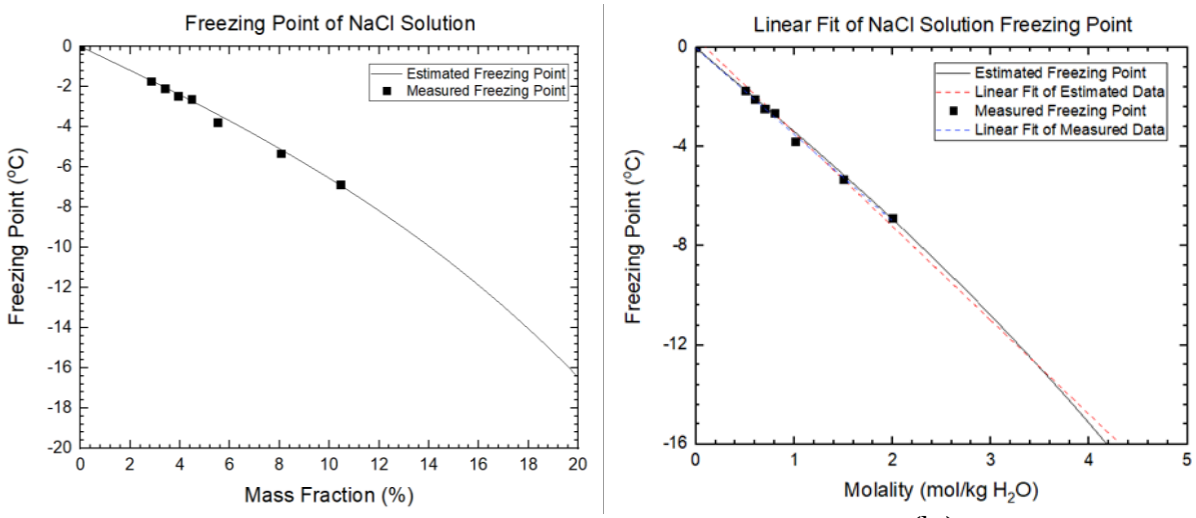

(a.) (b.)

Figure 20 Estimated and Measured Freezing Points of NaCl Solution

4.2.2 Prepared $CaCl_2$ Solution Freezing Points

Similarly, the $CaCl_2$ solutions are also prepared based on the concentrations listed in Section 3.3.2 Table 4. The tests for $CaCl_2$ solution freezing points are conducted. The real molality and the equivalent mass fractions of prepared $CaCl_2$ solutions are shown in Table 10; the estimated and measured freezing points and the deviations of $CaCl_2$ solutions are also listed. The estimated freezing points, which are obtained based on literature's data[78; 79], and the measured $CaCl_2$ freezing points are plotted in Figure 21.

Table 10 Freezing Points of Prepared $CaCl_2$ Solutions

Molality of Prepared Solution (mol/kg H2O)	Equivalent Mass Fraction (%)	Estimated Freezing Point (°C)	Measured Freezing Point (°C)	Deviation T_M-T_E (°C)
0	0	0	0	0
0.20	2.17	-1.036	-1.486	-0.450
0.50	5.258	-2.643	-3.044	-0.401
0.70	7.209	-3.775	-4.282	-0.507
1.00	9.990	-5.693	-6.714	-1.021
1.50	14.27	-9.723	-*	-
* Circulating bath temperature range cannot fulfil the subcooling requirement of freezing.				

Figure 21 (a.) and (b.) demonstrate the freezing point of $CaCl_2$ solution over mass fraction and molality. Also, linear fitting analysis is conducted and shown in Figure 21(b.). The slopes of the linear fits of estimated and measured data are approximately -7.60 and -6.49, respectively. The corresponding R^2 are 0.9813 and 0.9903, which indicates that the estimated data do not fit well.

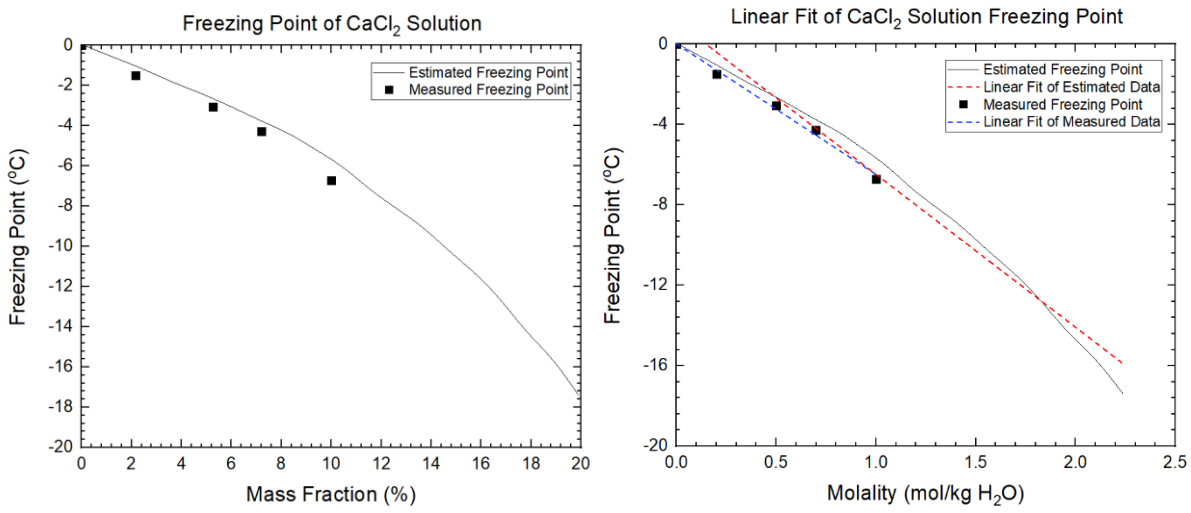

(a.) (b.)

Figure 21 Estimated and Measured Freezing Points of $CaCl_2$ Solution

4.2.3 Prepared $AlCl_3$ Solution Freezing Points

The $AlCl_3$ solutions are also prepared regarding the designed concentrations listed in Section 3.3.2 Table 4. As 99% purity $AlCl_3$ is dissolved for solutions, irritant gases are produced which the main component is hydrogen chloride. Therefore, molality 0.5, 0.71, and 1.18 mol/kg H_2O $AlCl_3$ solutions are prepared and diluted to other concentrations (molality 0.10, 0.20, and 0.35 mol/kg H_2O). The freezing point information of $AlCl_3$ solution is shown in Table 11, which only includes the real molality and equivalent mass fractions of prepared $AlCl_3$ solutions, and their corresponding measured freezing points. The measured freezing points are plotted over the mass fraction of solutions in Figure 22.

Table 11 Freezing Points of Prepared $AlCl_3$ Solutions

Molality of Prepared Solution (mol/kg H2O)	Equivalent Mass Fraction (%)	Estimated Freezing Point (℃) **	Measured Freezing Point (℃)	Deviation T_M-T_E (℃)
0	0	-	0	-
0.10	1.315	-	-1.071	-
0.20	2.597	-	-1.633	-
0.35	4.458	-	-3.610	-
0.50	6.249	-	-4.531	-
0.71	8.616	-	-6.911	-
1.18	13.63	-	-*	-

* Circulating bath temperature range cannot fulfil the subcooling requirement of freezing.

** Limited information about $AlCl_3$ solution freezing points, no reliable data supports

The measured freezing point of $AlCl_3$ solution over mass fraction and molality are shown in Figure 22 (a.) and (b.). Particularly, the linear fitting analysis is conducted for $AlCl_3$ solution

freezing point v.s. concentration in molality and plotted in Figure 22 (b.). The slope of the linear fit of measured data is approximately -9.64 and its corresponding R^2 is 0.9907.

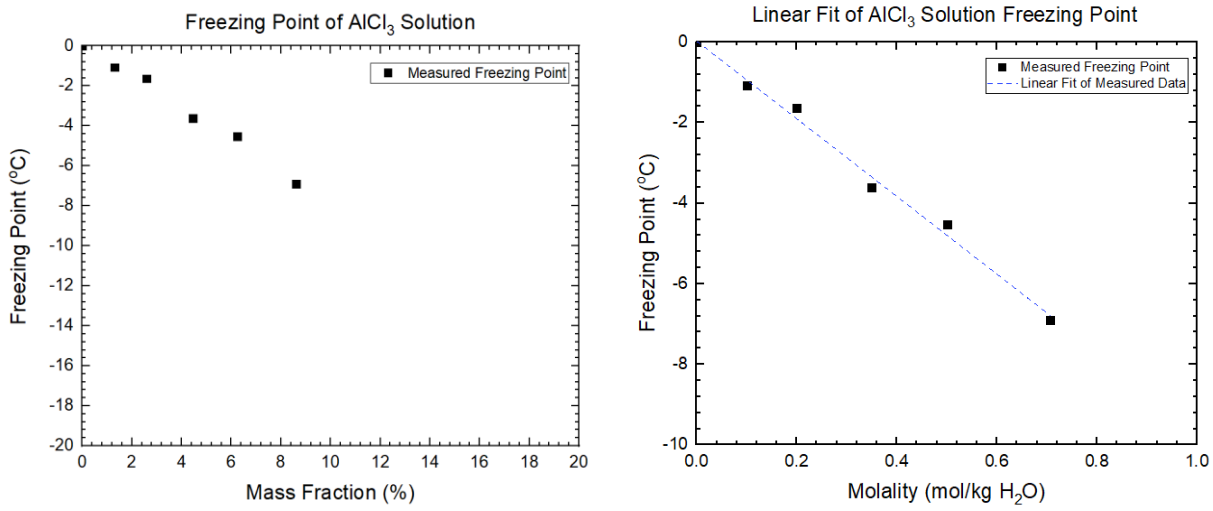

Figure 22 Measured Freezing Points of $AlCl_3$ Solution

4.2.4 Discussion of Freezing Point Test

As the freezing points of three types of salts in different concentrations are measured, the obtained temperatures are considered as the lower limit of the set-point for hydrate formation experiments. It is obvious that the freezing point of brine decreases with the increasing concentration, which is demonstrated in the graphs above. As is known, the salt is a kind of THI so that it can also be conjectured the phase equilibrium temperature of CP hydrates in brine reduces with the rising mass fraction.

Linear correlations of measured salt freezing point and molality can be discovered from the experiments, which could be explained by freezing point depression model[83] (Equation 9).

$$T_{FP} = T_{solvent} - T_{solute} = T_{solvent} - iK_f b$$

Equation 9 Freezing Point Depression Model

where, T_{FP} is the estimated freezing point of the solution, ℃; $T_{solvent}$ is the freezing point of the solvent (DI water), which is 0℃; T_{solute} is the depressed temperature caused by a solute (salt), ℃; i is the van't Hoff factor[84; 85], which represents the ratio between the actual concentration of particles dissolved in solvent and concentration of particles in the solid substance; K_f is the freezing point depression constant, which is normally regarded to be 1.86 ; and b is the solute (salt) molality, mol/kg H_2O.

However, the measured brine freezing points obtained in this project and the temperature data found in the literature do not exactly match the depression model. The results presented in Table 12 indicate that the other factors exist which affect the freezing point of the electrolytes.

Table 12 Details of Linear Fit Slopes

Category	Ideal van't Hoff Factor	Estimated Slope, S_{Est}	Slope of Linear Fitting, $S_{Measured}$	Deviation, $\|S_{Est}\| - \|S_{Measured}\|$
NaCl	2	-3.72	-3.49	0.23
$CaCl_2$	3	-5.58	-6.49	-0.91
$AlCl_3$	4	-7.44	-9.64	-2.20

Also, the measurement errors exist even repetition tests have been done. Particularly, more than one test has been conducted on measuring the freezing points of DI water and NaCl solutions (0.5 mol/kg H_2O, 0.6 mol/kg H_2O). The repeated test results show that experimental errors for freezing point test could be 0.2℃ - 0.5℃.

4.3 Observations of Hydrate Formation Acceleration Tests

4.3.1 Effects of Intermittent Stirring

In this project, the experiments of hydrate formation are stirred intermittently to accelerate the nucleation progress. Although the induction times of the experiments are stochastic, the observations from the tests conducted with the same amount of CP and salt solution under the same conditions confirm from a side the positive effect of agitation. From the experiments, some observations are listed as following:

1) The CP hydrate film appears earlier in the test tubes which agitation is applied than the others under the static state;
2) The hydrate grows quicker under the agitation condition than the static condition so that the time required for completing the hydrate formation process is reduced;
3) The induction time may last the whole night and no crystal appears, while the nucleation process could start within one hour when an agitation introduced.

As the findings discussed are noticed from the hydrate formation process, the contingency and uncertainty of these observations inevitably exist. Therefore, the experiments in this project cannot radically prove that CP hydrate formation is accelerated by stirring the liquid; but can be regarded as a reference for shortening the hydrate formation process.

4.3.2 Effects of CP and Solution Ratio

As mentioned in Section 3.4.4.2, the CP hydrate formation experiments with DI water are conducted to select the ratio of CP and salt solution. The photos taken for the completed hydrate formation tests are shown in Figure 23 and Figure 24, which are conducted under the static state.

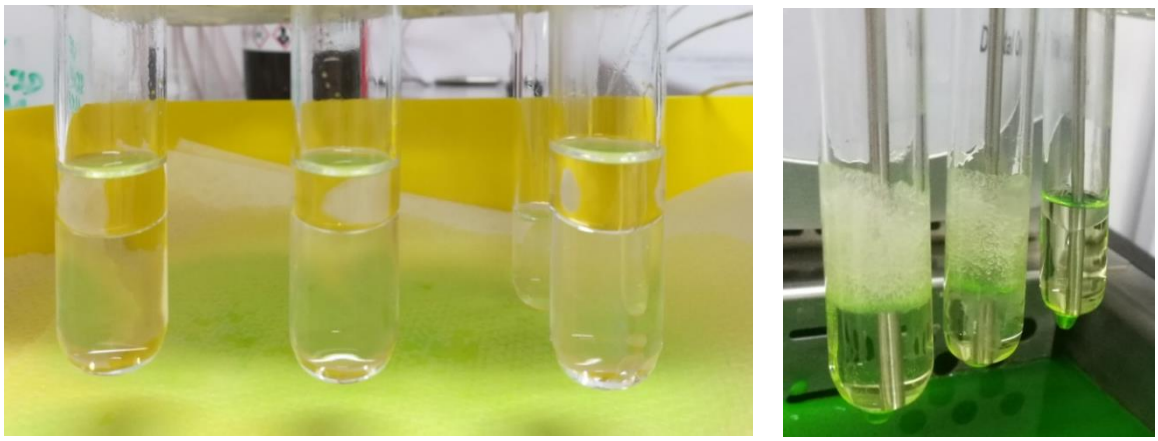

(a.) (b.)

Figure 23 CP Hydrate Formation Experiment with DI Water (@Volumetric CP: Water = 1:3)

The prepared test tubes with CP and DI water are shown in Figure 23 (a.), and the completed hydrate formation result of this test is attached as Figure 23 (b.). From Figure 23 (b.), a large amount of water is retained at the bottom of the tubes and a little hydrate formed since the CP is entirely converted to the hydrate. Particularly, the ratio of CP and DI water remained in the third test tube from the left, which no hydrate appears, is much lower than 1:3 due to the volatility of CP. Therefore, the excess CP is required to avoid negative impacts of volatilization.

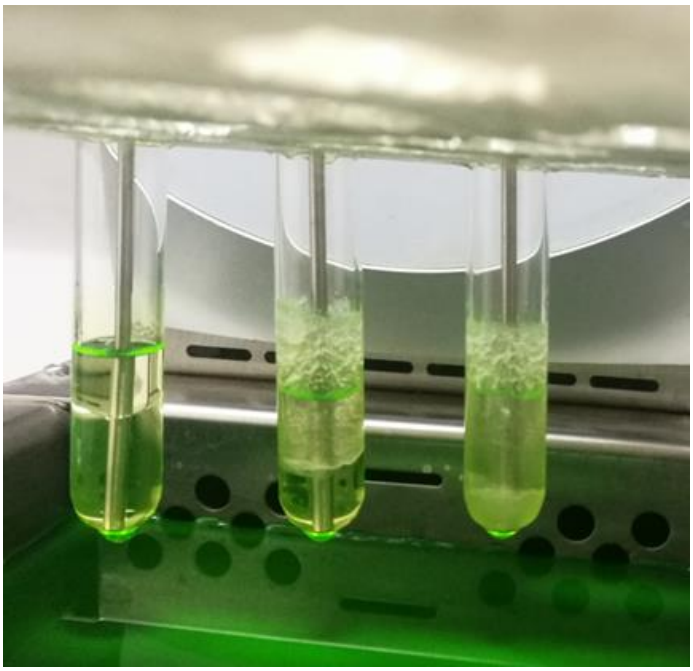

Figure 24 Completed CP Hydrate Formation Experiments with Different Volumetric Ratios of CP and DI Water (1:1, 2:1, and 3:1)

Figure 24 shows the completed CP hydrate formation tests with different ratio of CP and DI water, which are 1:1, 2:1, and 3:1 in sequence. The experiment is also conducted under static conditions. The observed results demonstrate that the test with the volumetric ratio CP: DI water = 2:1 has a better performance than the other two tests. Thus, ratio 2:1 is chosen for the next experiments. The possible speculation could be proposed that the CP hydrate formation process may be accelerated by increasing the amount of CP to some extent.

4.3.3 Effects of Subcooling

As the subcooling is the key driving force for this project, the hydrate formation rate can be significantly affected by the subcooling. It can be found that the less induction time required for the tests with higher subcooling level than the tests with lower subcooling level.

Similarly, this result could not be radically proved by this project, but the observations of the tests are aligned with the findings from the literature[40; 86] which can support the experiments designed for this thesis. For this project, as the measured freezing point of each prepared salt solution is summarized in Section 4.2, the bath temperature of the cryostat is designed just above the brine freezing points to maximise the subcooling and reduce the negative impacts of solution freeze.

4.4 Observations of Hydrate Formation Process

The hydrate formation experiments are conducted after completing the preliminary experiments of calibration tests and freezing point tests. The CP hydrate formation process can be observed visually during the experiments. Some photos captured during the formation process are shown as follows.

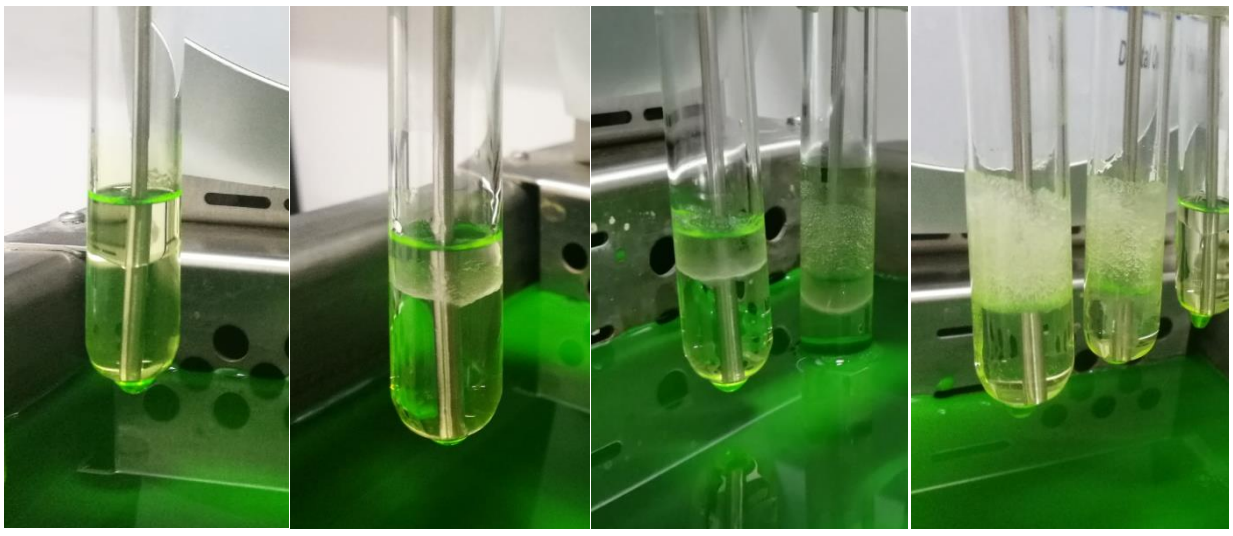

(a.) (b.) (c.) (d.)

Figure 25 Observations of CP Hydrate Formation Process (@Volumetric CP: Water = 1:3)

Figure 25 demonstrates main observations of the hydrate formation process, which is conducted with CP and DI water at a volumetric ratio of 1:3 (stoichiometric ratio 1:17) under the static state. Figure 25 (a.) is the initial condition of the experiment which is during the induction time. No hydrate or crystal appears at the beginning of the formation process. After a long period of induction, the hydrate appears at the interface of CP and water phases (As shown in Figure 25 (b.)). The hydrate grows from the interface to the bulk area and along the wall of the test tubes (Figure 25 (c.)). The hydrate formation ends when either CP or DI water is completely consumed (Figure 25 (d.)). In this test, the CP is entirely converted to the CP hydrate and the excess water remained at the bottom of the test tube.

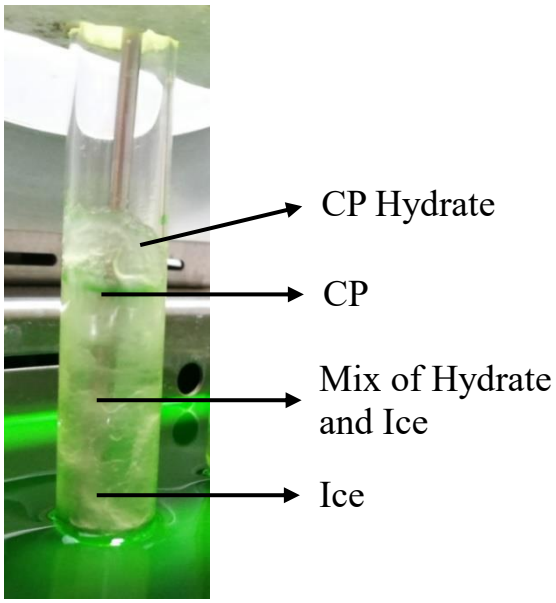

Figure 26 Completed Hydrate Formation under Stirring Condition

A completed CP hydrate formation test is shown in Figure 26. The experiment is carried out under the stirring conditions. The components of the mix in the test tube are pointed out since the CP hydrate and ice could be distinguished by eyes. A small amount of solution may crystallize during the hydrate formation process and mix with CP hydrates. The agitation enhances the hydrate formation process but also blend the components inside the test tubes.

4.5 Observations of Hydrate Dissociation Process

Based on the hydrate formation experiments, the dissociation experiments can be conducted when a sufficient amount of hydrate formed. The excess CP or solution is removed before the dissociation process to reduce the possible impacts on equilibrium temperature measurement. The photos attached below are captured during the dissociation processes of the experiments done for this thesis. Figure 27 (a.-b.), Figure 27 (c.-d.), and Figure 27(e.) are selected from three CP hydrate dissociation tests which have a better appearance for observation discussion.

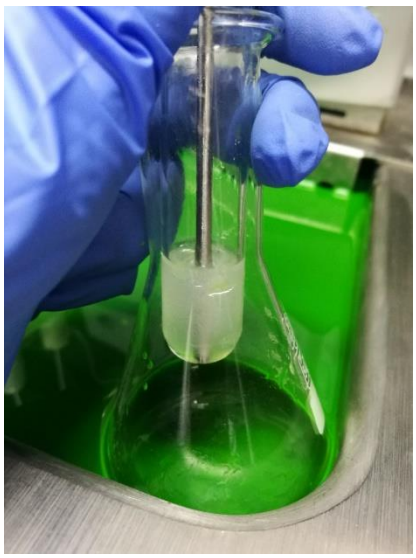

(a.)

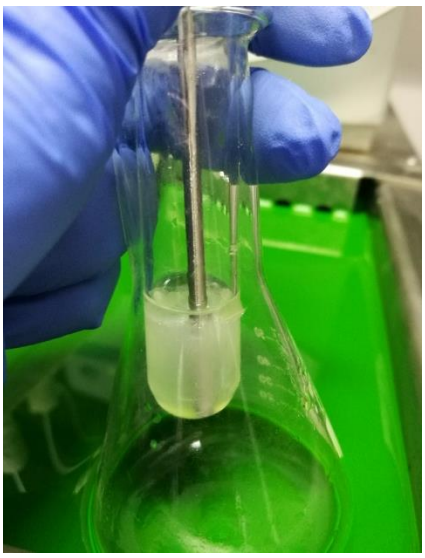

(b.)

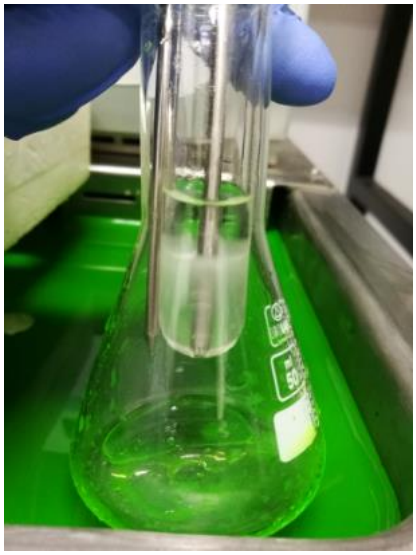

(c.)

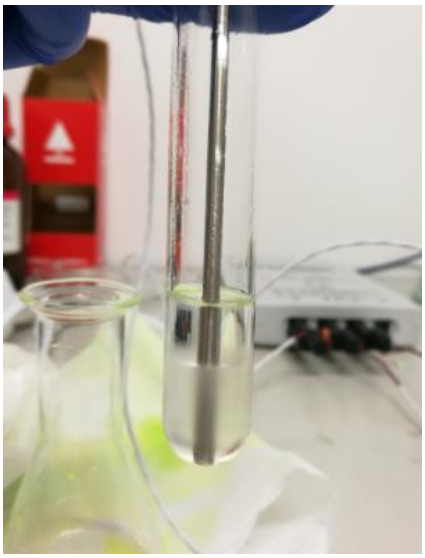

(d.)

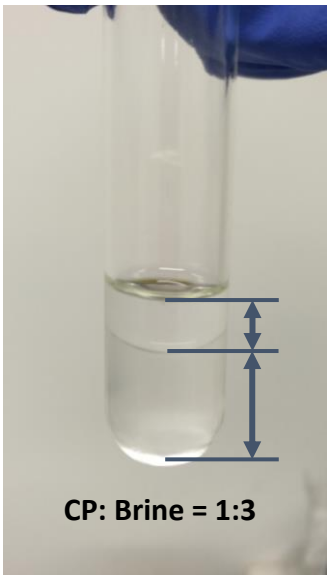

(e.)

Figure 27 Observations of CP Dissociation Process

Figure 27 (a.-e.) demonstrates the typical phenomena of quick CP hydrate dissociation process. As mentioned in Section 3.4.6, the test tubes for hydrate dissociation experiments are taken out from the circulating bath and placed in a conical flask, which is put at the surface of coolant to reduce the temperature difference between hydrates and external environment.

Figure 27 (a.) shows the initial condition of dissociation experiment. The dissociation can be observed visually at the interface of CP and CP hydrate as shown in Figure 27 (b.). Small "bubbles", which is actually the small CP hydrate crystals, rise from the lower part of the mix towards the CP phase and dissociate into CP and salt solution at the interface.

With the progressing of dissociation, the remained CP hydrates gather at the interface of two phases. In the test tube, the liquid at the top phase is CP and the other phase is the mix of hydrates and brine. Particularly, the dissociated salt solution is at the bottom of the tube (Figure 27 (c.)). Seen from Figure 27 (c.-d.), the CP phase is clear and transparent, whereas the solution phase is turbid due to the undissociated hydrates. The dissociation process is regarded as completed when few hydrates remain in test tubes. Figure 27 (e.) illustrates the final stage of CP hydrate dissociation experiment, it can be observed that the CP and brine ratio of well-dissociated CP hydrates is approximately 1:3 as shown in the photo.

4.6 Results of Data Processing

As the measured temperature data are collected and progressed. The results of data processing are demonstrated and discussed in this section.

4.6.1 Monitored Temperature Data of Hydrate Formation and Dissociation Process

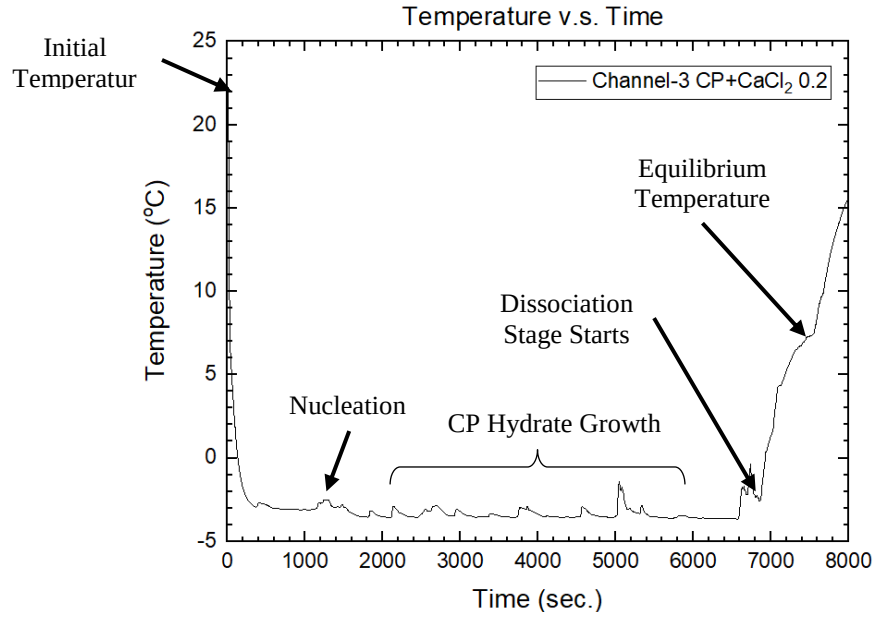

Figure 28 Monitored Temperature Data of the Experiment v.s Time (CP+$CaCl_2$@0.2 mol/kg H_2O)

One of the monitored temperature data for CP hydrate formation and dissociation process is illustrated in Figure 28. The plotted data have a similar tendency to Ho-Van's study mentioned in Section 2.1.4. The fluctuations appear during the growth process are mainly caused by intermittent stir and the observation actions. The dissociation experiments start by taking out the test tube from the bath and the detected temperature increases rapidly. It can be seen from the graph that the increasing temperature slows down during the hydrate dissociation process due to the endothermic dissociation process, which indicates the existence of CP hydrates. A sudden increase of the monitored temperature represents the end of hydrate dissociation stage as shown in Figure 28. Therefore, the phase equilibrium temperature of CP hydrates can be obtained from both visual observation and graph analysis.

4.6.2 Measured Phase Equilibrium Temperatures

The measured phase equilibrium temperatures of CP hydrate formation in different brine are presented as follows. As the quick dissociation method is applied in this thesis, the highly accurate phase equilibrium temperatures cannot be obtained. It is possibly due to the small dose level experiments conducted since the small samples may be significantly affected by the external environment. The disturbances could be introduced to the system by manual operations, e.g. intermittent agitation and observation actions.

4.6.2.1 Measured Data of Phase Equilibrium Temperature of CP Hydrate in NaCl Solution

Ionic strength (*I*) is the total ion concentration in the solution which is calculated with the *Debye-Hückel Limiting Law* proposed by Peter Debye and Erich Hückel in 1923[87; 88]. The mathematical formula for ionic strength is shown as Equation 10.

$$I = \frac{1}{2}\sum_{i}^{n} c_i {z_i}^2$$

Equation 10 Mathematical Formula for Ionic Strength

where I is the ionic strength, mol/kg H_2O; c_i is the molar concentration of ion i, mol/L; z_i is the charge number of ion i. Detailed calculations are shown in APPENDIX-F. As DI water is used as a solvent, the molar concentration of ion can be approximated to the molality value.

The concentrations and measured equilibrium temperature of CP hydrate are listed in Table 13, which also includes the effective mole fraction and ionic strength of the brine.

Table 13 Concentrations and Measured Equilibrium Temperature of CP Hydrate in NaCl Solution

Molality (mol/kg H_2O)	Equivalent Mass Fraction (%)	Effective Mole Fraction	Ionic Strength	Equilibrium Temperature (°C)
0	0	0	0	7.7
0.50	2.839	0.0177	0.50	6.126
0.70	3.931	0.0246	0.70	5.030
1.01	5.587	0.0352	1.01	4.378
1.50	8.060	0.0512	1.50	2.532

4.6.2.2 Measured Data of Phase Equilibrium Temperature of CP Hydrate in $CaCl_2$ Solution

Similarly, the concentrations and measured equilibrium temperature of CP hydrate in $CaCl_2$ solution are listed in Table 14.

Table 14 Concentrations and Measured Equilibrium Temperature of CP Hydrate in $CaCl_2$ Solution

Molality (mol/kg H_2O)	Equivalent Mass Fraction (%)	Effective Mole Fraction	Ionic Strength	Equilibrium Temperature (°C)
0	0	0	0	7.7
0.20	2.170	0.0142	0.60	6.725
0.50	5.258	0.0351	1.50	5.365
0.70	7.209	0.0486	2.10	4.738
1.00	9.990	0.0683	3.00	2.647

4.6.2.3 Measured Data of Phase Equilibrium Temperature of CP Hydrate in $AlCl_3$ Solution

The concentrations and measured equilibrium temperature of CP hydrate in $AlCl_3$ solution are also presented in Table 15.

Table 15 Concentrations and Measured Equilibrium Temperature of CP Hydrate in $AlCl_3$ Solution

Molality (mol/kg H_2O)	Equivalent Mass Fraction (%)	Effective Mole Fraction	Ionic Strength	Equilibrium Temperature (°C)
0	0	0	0	7.7
0.10	1.315	0.0107	0.60	6.953
0.20	2.597	0.0213	1.20	6.750
0.35	4.458	0.0369	2.10	6.401
0.50	6.249	0.0521	3.00	5.605
0.71	8.616	0.0727	4.24	4.397

4.6.2.4 Graphs of Measured Phase Equilibrium Temperature v.s. Concentrations

Based on the experimental data listed in Table 13, Table 14 and Table 15, the relationships of the measured CP hydrate phase equilibrium temperature and concentrations are plotted in the scatter graph (shown from Figure 30 to Figure 32).

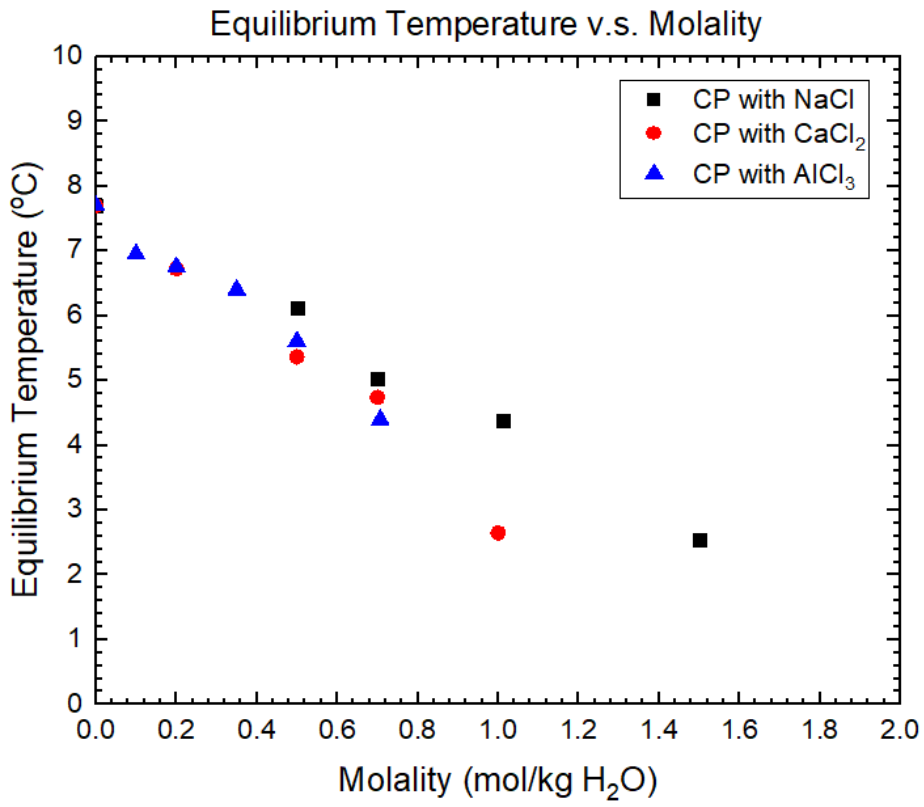

Figure 29 Equilibrium Temperature of CP Hydrate v.s. Molality of Salt Solution

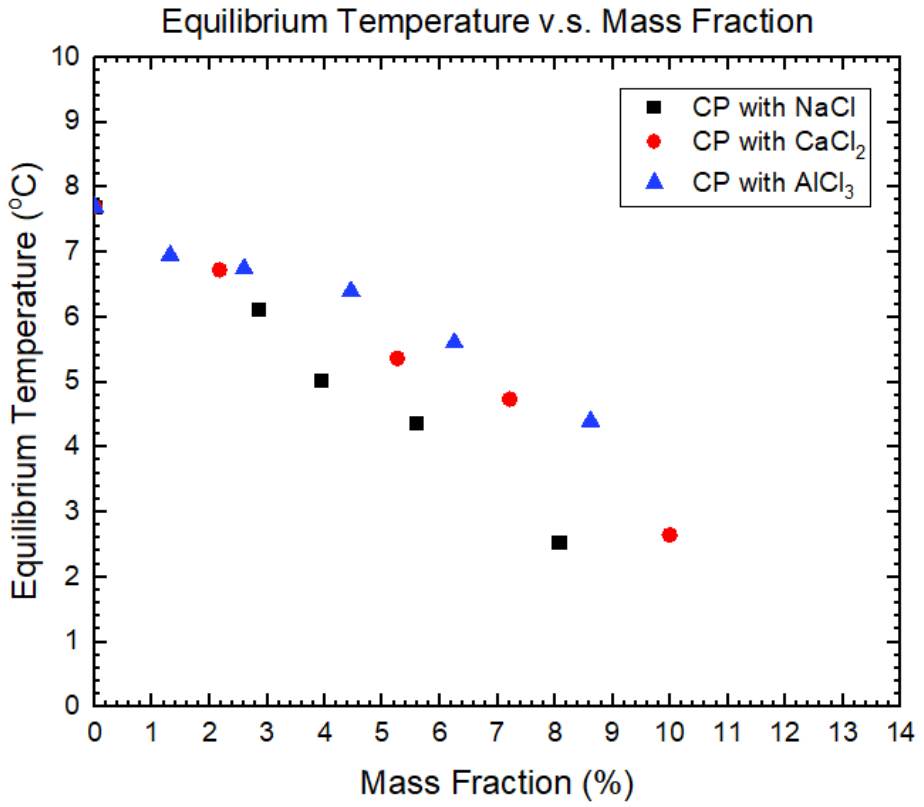

Figure 30 Equilibrium Temperature of CP Hydrate v.s. Mass Fraction of Salt Solution

Equilibrium Temperature v.s. Effective Mole Fraction

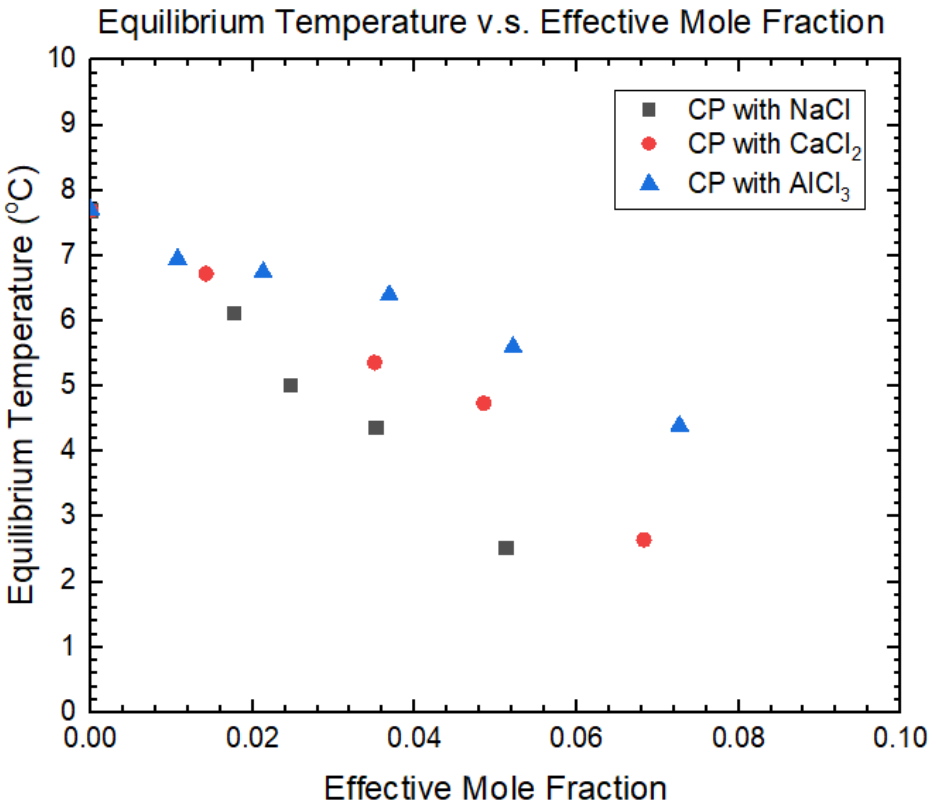

Figure 31 Equilibrium Temperature of CP Hydrate v.s. Effective Mole Fraction of Salt Solution

Equilibrium Temperature v.s. Ionic Strength

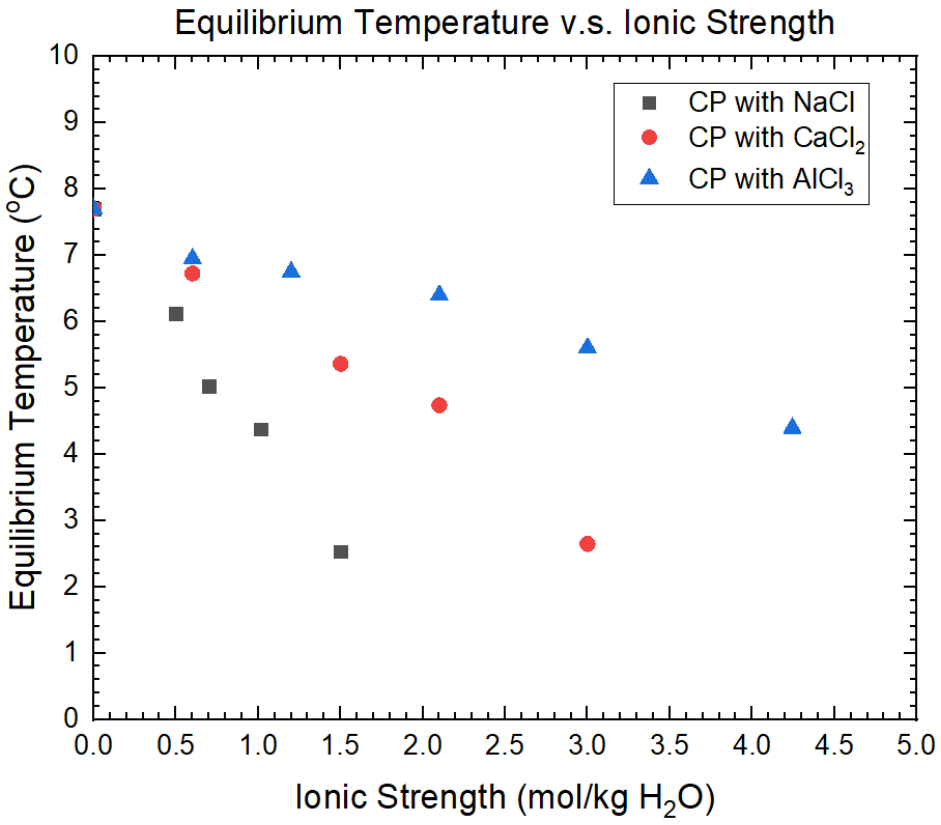

Figure 32 Equilibrium Temperature of CP Hydrate v.s. Ionic Strength of Salt Solution

4.6.2.5 Discussions of Equilibrium Temperature Graphs

The graphs above demonstrate that the equilibrium temperature of CP hydrates decreases with the increasing concentration of salt concentration (Figure 29 and Figure 30). As NaCl, $CaCl_2$, and $AlCl_3$ solutions used in this project are strong electrolytes, the relationships between equilibrium temperature and effective mole fraction, equilibrium temperature and ionic strength are considered and analysed (Figure 31 and Figure 32). From Figure 30 to Figure 32, it can be observed that the NaCl solution has a higher-level impact on hydrate equilibrium temperature than the other salts at the same concentration (mass fraction, effective mole fraction, and ionic strength), whereas the effect of $AlCl_3$ solution is the lowest compared with the other two salts.

Based on the Hu-Lee-Sum correlation mentioned in Section 2.4 Equation 1:

$$\frac{\Delta T}{T_0 T} = -\frac{nR}{\Delta H_{diss}} \times \ln a_w = C_1 X + C_2 X^2 + C_3 X^3$$

The $\Delta T / T_0 T$ is plotted over the effective mole fraction and presented in Figure 33.

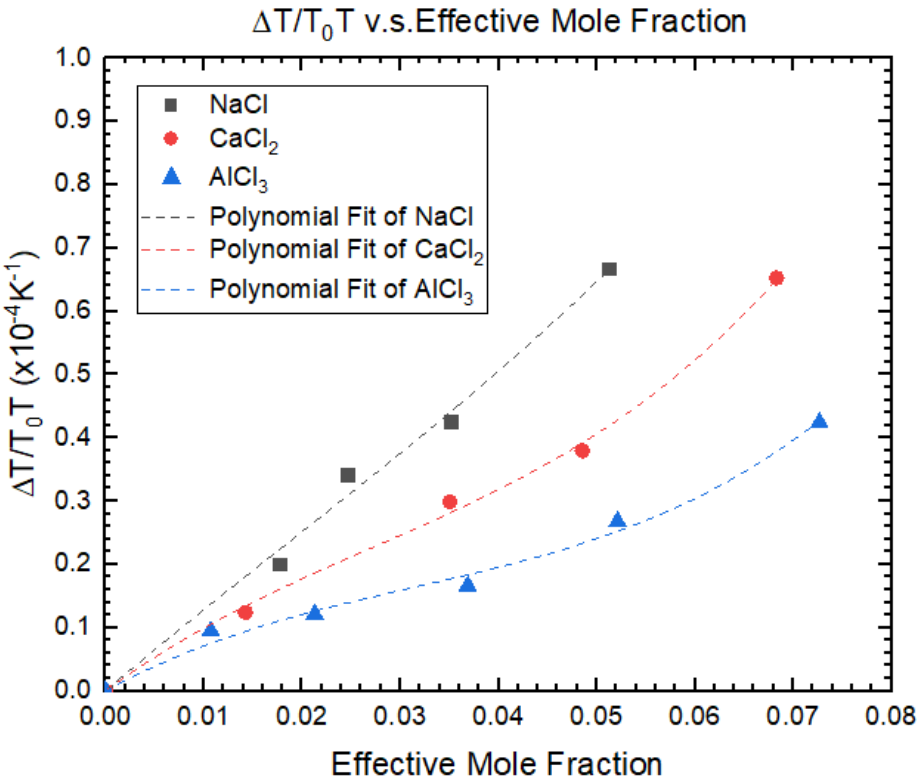

Figure 33 Plotting Based on Hu-Lee-Sum Correlation

Other fitting analyses are also conducted for $\Delta T / T_0 T$ v.s. effective mole fraction, while the results of fitting show that the thrice polynomial fitting has the best performance, which each curve aligns with the Hu-Lee-Sum correlation; while the concatenate fitting for all scattered data do not fit the thrice polynomial well. Possible reasons include:

- The effective mole fraction of experiments conducted are within the range 0 ~ 0.08 so that the experimental data could not represent the global results;
- As n is the hydration number which represents the water required for one molar hydrate forms, the $-nR/\Delta H_{diss}$ value is regarded as a constant when the cavities of hydrate are fully occupied by guest gas; otherwise, the n is higher than the value of fully occupied value ≈17 for sII hydrates;
- Measurement errors are inevitable which may lead to significate deviations.

The correlation between $\ln a_w$ and effective mole fraction of each electrolyte can be obtained when the $-nR/\Delta H_{diss}$ value is confirmed. That is, the water activity a_w can be calculated with the mathematical Equation 11.

$$\ln a_w = -\frac{\Delta H_{diss}}{nR}(C_1X + C_2X^2 + C_3X^3) = B_1X + B_2X^2 + B_3X^3$$

Equation 11 Hu-Lee-Sum Correlation for Water Activity

The details for the thrice polynomial fitting is listed in Table 16.

Table 16 Details for Polynomial Fitting in Figure 33

Category	C_1	C_2	C_3	R^2
NaCl	13.262	-52.171	913.464	0.9976
$CaCl_2$	11.425	-169.763	2076.180	0.9992
$AlCl_3$	8.518	-157.414	1665.443	0.9967

Considering the mathematical formulas for effective mole fraction and ionic strength (Equation 2 and Equation 10). The relationship between effective mole fraction and the ionic strength is deduced in APPENDIX-G. A linear correlation exists between the reciprocal of effective mole fraction and the reciprocal of ionic strength.

Since the molality values are relatively low compared with the mole of 1 kg DI water, the relationship between effective mole fraction and ionic strength can be considered as linear, which is explained in APPENDIX-G. So, the relationship between $\Delta T/T_0T$ and ionic strength can also be obtained with a thrice polynomial fitting result (shown in Figure 34 and Table 17).

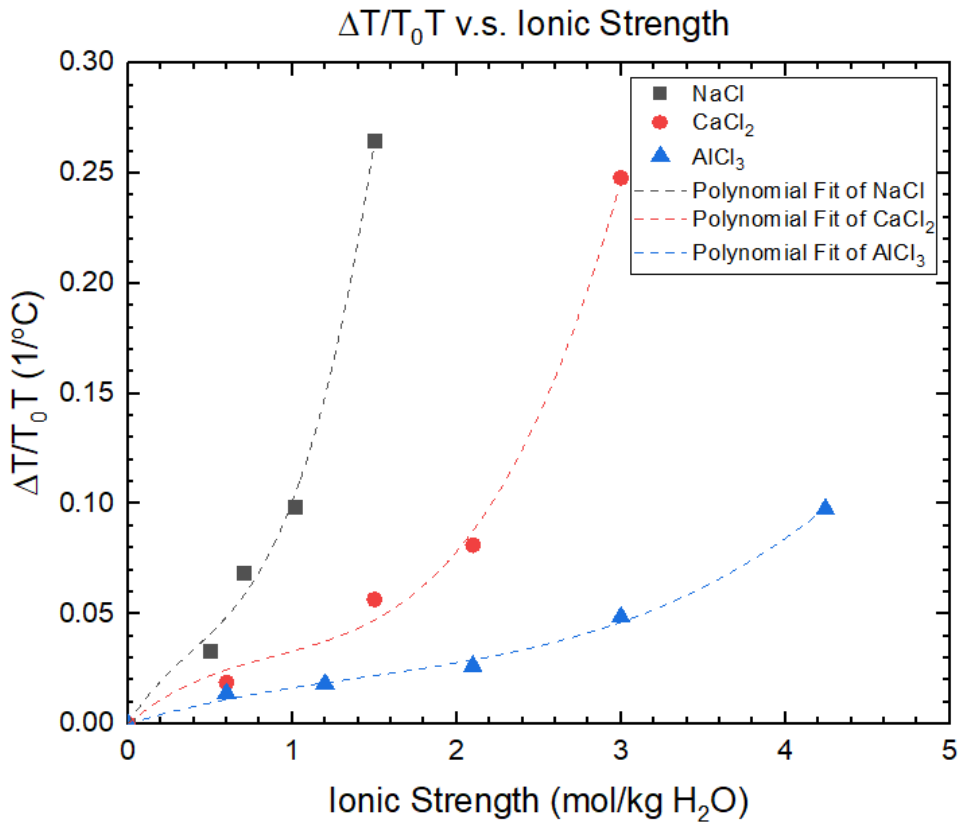

Figure 34 Plotting with Ionic Strength

Table 17 Details for Polynomial Fitting in Figure 34

Category	c_1	c_2	c_3	R^2
NaCl	0.4785	-0.0822	0.0393	0.9976
$CaCl_2$	0.2697	-0.0912	0.0245	0.9992
$AlCl_3$	0.1481	-0.0459	0.0082	0.9965

4.6.3 Comparison of Measured Data with Literature

The measured phase equilibrium temperature of CP hydrate in NaCl solution is compared with the data from literature[31; 89; 90]. The comparison graph is shown in Figure 35, which illustrates that the experiment results are aligned with the equilibrium temperature data from the literature.

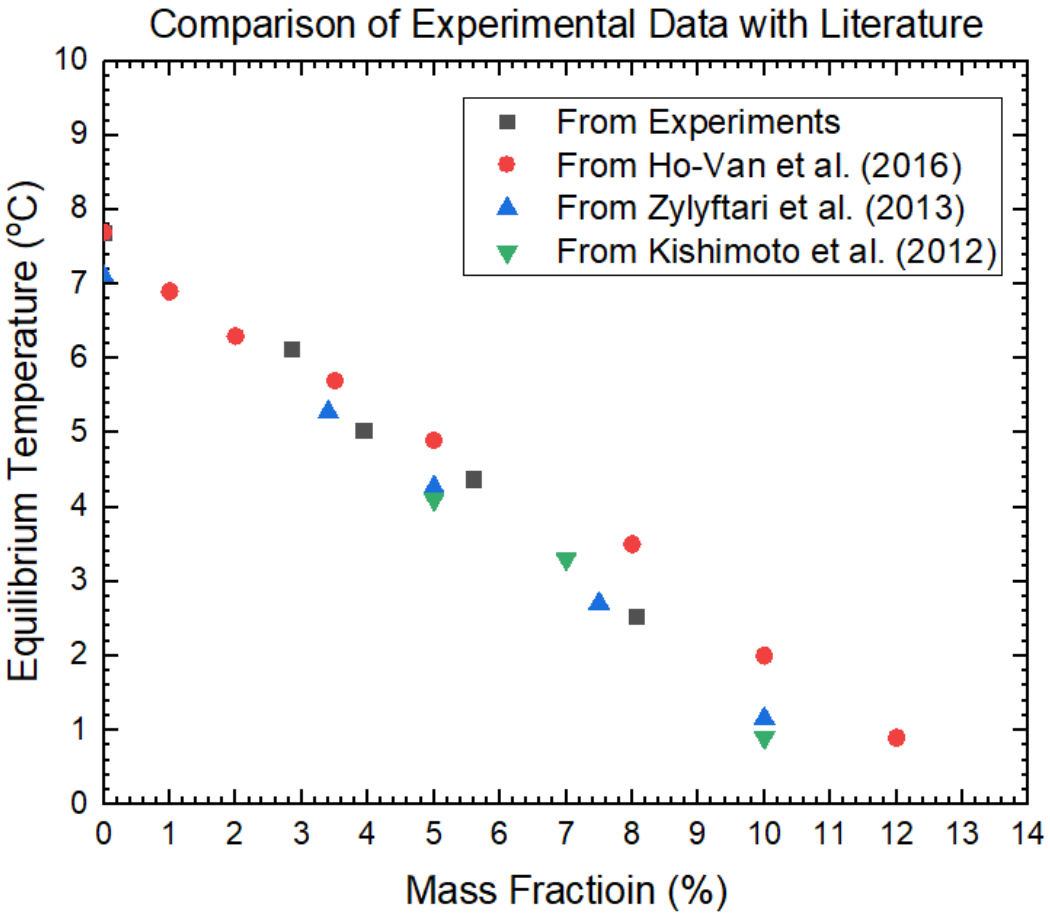

Figure 35 Comparison of Measured Phase Equilibrium Temperature with Data from Literature (NaCl Solution)

Chapter 5: Conclusion and Future Works

5.1 Comprehensive Conclusion

In this thesis, the phase equilibrium temperature of CP hydrates in three types of electrolytes has been investigated at a small dose level by conducting the hydrate formation process experiment and quick dissociation experiment. Some preliminary experiments are designed for supporting the formation and dissociation experiments.

The conclusions for the thesis are summarized below.

The experiments are conducted with approximately 2mL salt solution and 4mL CP, which are easy to operate and convenient to observe. Less time required for completing each test compared with a relatively larger scale test. Also, multiple tests can proceed simultaneously.

The hydrate formation and dissociation processes are observed visually by simply taking out the test tubes from the cryostat during the experiments. The hydrate formation and dissociation happen at the interface of two phases, which is aligned with the literature.

The phase equilibrium temperature of CP hydrates can be obtained during the hydrate dissociation process. The experimental data are confirmed with two approaches:

1) The monitored temperature is the CP hydrate equilibrium temperature when few hydrate particles left in the test tube, which can be directly observed by eyes;
2) The CP hydrate equilibrium temperature is detected at the point where a sharp increase of monitored temperature appears during the dissociation process.

Experimental data of CP hydrate phase equilibrium temperature are measured with a quick dissociation method in this project. This quick method requires much less time than a slower method which may take a few days for each test. However, this method could not provide very accurate equilibrium data, due to the rapid increases of monitored temperature caused by the huge temperature difference between the hydrates and air. Additionally, the small dose experiments are easily affected by the external conditions so that uncertainty and measurement error is inevitable. Therefore, the data obtained in this project can provide a possible range of the actual equilibrium temperature which can be measured with the slower dissociation method.

The equilibrium temperatures of CP hydrates in NaCl, $CaCl_2$ and $AlCl_3$ solutions at different molality are measured and presented in this thesis, which is summarized in previous sections.

Based on the molality, the equivalent mass fraction, effective mole fraction, and ionic strength are calculated with the mathematic formulas. Thus, the analyses on the relationship between hydrate equilibrium temperatures and concentrations (molality, mass fraction, effective mole fraction, ionic strength) are conducted by scatter plot. The graphs clearly demonstrate that the hydrate equilibrium temperature decreases with the increasing concentrations; and the effect level of three electrolytes at the same mass fraction is NaCl > $CaCl_2$ > $AlCl_3$ solutions.

The analysis of $\Delta T/T_0 T$ v.s. effective mole fraction and $\Delta T/T_0 T$ v.s. ionic strength is conducted considering the Hu-Lee-Sum correlation. The thrice polynomial fitting results show the experimental data of each salt align with this correlation proposed in others' article, so that the water activity can further be deduced. However, the concatenate fitting of all three salts do not fit well, possibility due to the limitations of the experiments which have been discussed in the previous section.

5.2 Recommendations for Future Works

Since the quick CP hydrate dissociation method is applied for this thesis, the rough data of CP hydrate phase equilibrium temperatures are measured from the experiments. Some future studies are recommended as follows:

- A slower hydrate dissociation process is necessary to conduct to obtain a more accurate hydrate equilibrium temperature for further study;
- The broader electrolyte concentration range and more types of inorganic salts should be considered to figure out the global relationship between equilibrium temperature and concentrations, and between the water activity and effective mole fraction;
- The relationships between cyclopentane hydrate nucleation rate and effective mole fraction (or water activity) are researched with different electrolytes (for example, sodium chloride, potassium chloride, calcium chloride, magnesium chloride, and aluminium chloride) at different concentrations with constant subcooling provided, other single or mixed inorganic salt solutions may also be considered.

Other recommendations for improving the current experiments:

- Increasing the experimental repetition times to reduce the uncertainty and contingency of the measured results so that the accuracy can be improved to some extent, although the modified measurement still could not provide the exact equilibrium temperature;
- Modify the experiment by implementing automatic agitation instead of manual operation to avoid introducing disturbances to the system.

Reference

[1] Ritchie, H., & Roser, M. (2018). Fossil Fuels. *OurWorldInData.org*. Retrieved from 'https://ourworldindata.org/fossil-fuels' [Online Resource]

[2] Factbook, T. W. (2017). Country Comparison :: Natural Gas - Proved Reserves. Retrieved from https://www.cia.gov/library/publications/the-world-factbook/rankorder/2253rank.html

[3] Zifan, A. (2014). Countries by natural gas proven reserves (2014), based on data from The World Factbook. In.

[4] Birol, F., Corben, J., Argiri, M., Baroni, M., Corbeau, A.-S., Cozzi, L., & Cronshaw, I. (2011). *Are we entering a golden age of gas?*

[5] Taylor, C. E., & Kwan, J. T. (2004). *Advances in the Study of Gas Hydrates*: Springer US: Boston, MA.

[6] Demirbas, A. (2010). *Methane Gas Hydrate*: London : Springer London.

[7] Du, J., Li, H., & Wang, L. (2014). Effects of ionic surfactants on methane hydrate formation kinetics in a static system. *Advanced Powder Technology, 25*(4), 1227-1233.

[8] Veluswamy, H. P., Wong, A. J. H., Babu, P., Kumar, R., Kulprathipanja, S., Rangsunvigit, P., & Linga, P. (2016). Rapid methane hydrate formation to develop a cost effective large scale energy storage system. *Chemical Engineering Journal, 290*, 161-173.

[9] Du, J., Li, H., & Wang, L. (2018). Cooperative effect of surfactant addition and gas-inducing agitation on methane hydrate formation rate. *Fuel, 230*, 134-137.

[10] Chong, Z. R., Yang, S. H. B., Babu, P., Linga, P., & Li, X.-S. (2016). Review of natural gas hydrates as an energy resource: Prospects and challenges. *Applied Energy, 162*, 1633-1652.

[11] Li, H., & Wang, L. (2015). Hydrophobized particles can accelerate nucleation of clathrate hydrates. *Fuel, 140*, 440-445.

[12] Koh, C., Westacott, R., Zhang, W., Hirachand, K., Creek, J., & Soper, A. (2002). Mechanisms of gas hydrate formation and inhibition. *Fluid Phase Equilib., 194*, 143-151.

[13] Boswell, R., Yamamoto, K., Lee, S.-R., Collett, T., Kumar, P., & Dallimore, S. (2014). Chapter 8 Methane Hydrates. In T. Letcher & T. M. Letcher (Eds.), *Future energy : improved, sustainable and clean options for our planet* (pp. 159-178): Elsevier Ltd.

[14] Sloan, E. D. (2003). Fundamental principles and applications of natural gas hydrates. *Nature, 426*(6964), 353.

[15] Yin, Z., Khurana, M., Tan, H. K., & Linga, P. (2018). A review of gas hydrate growth kinetic models. *Chemical Engineering Journal, 342*, 9-29.

[16] Chen, D., Xu, W., & Zhao, Z. (2001). Gas hydrate structure and hydration numbers and its densities. *Acta Mineralogica Sinica, 2*.

[17] Sloan, E. D., & Koh, C. A. (2007). *Clathrate hydrates of natural gases*: CRC press.

[18] Hu, Y., Lee, B. R., & Sum, A. K. (2018). Universal correlation for gas hydrates suppression temperature of inhibited systems: II. Mixed salts and structure type. *AIChE Journal, 64*(6), 2240-2250.
[19] NaturalGas.org. (2014). Background of Natural Gas. Retrieved from https://web.archive.org/web/20140709040340/http://naturalgas.org/overview/background/
[20] Maslin, M., Owen, M., Betts, R., Day, S., Jones, T. D., & Ridgwell, A. (2010). Gas hydrates: past and future geohazard? *Philosophical Transactions of the Royal Society of London A: Mathematical, Physical and Engineering Sciences, 368*(1919), 2369-2393.
[21] Board, O. S., & Council, N. R. (2004). *Charting the future of methane hydrate research in the United States*: National Academies Press.
[22] Fan, S., & Hua, B. (2005). Research Progress of Natural Gas Hydrate Storage and Transportation Technology. *Natural Gas Industry, 25*(11), 100-103.
[23] Makogon, Y., & Holditch, S. A. (2002). *Gas Hydrates as a Resource and a Mechanism for Transmission*. Paper presented at the SPE Annual Technical Conference and Exhibition, San Antonio, Texas.
[24] Agency, I. E. (2016). *Energy and Air Pollution*.
[25] Agency, I. E. (2016). *World Energy Outlook 2016*.
[26] Agency, C. I. (2018). The World Factbook. 'https://www.cia.gov/library/publications/resources/the-world-factbook/geos/xx.html' [Online Resource]
[27] Milkov, A. V. (2004). Global estimates of hydrate-bound gas in marine sediments: how much is really out there? *Earth-Science Reviews, 66*(3), 183-197.
[28] Chong, Z. R., Chan, A. H. M., Babu, P., Yang, M., & Linga, P. (2015). Effect of NaCl on methane hydrate formation and dissociation in porous media. *Journal of Natural Gas Science and Engineering, 27*, 178-189.
[29] Mimachi, H., Takeya, S., Gotoh, Y., Yoneyama, A., Hyodo, K., Takeda, T., & Murayama, T. (2016). Dissociation behaviors of methane hydrate formed from NaCl solutions. *Fluid Phase Equilibria, 413*, 22-27.
[30] Ho‐Van, S., Bouillot, B., Douzet, J., Babakhani, S. M., & Herri, J. M. (2018). Experimental measurement and thermodynamic modeling of cyclopentane hydrates with NaCl, KCl, CaCl2, or NaCl‐KCl present. *AIChE Journal, 64*(6), 2207-2218.
[31] Ho-Van, S., Douzet, J., Le-Quang, D., Bouillot, B., & Herri, J.-M. (2016). *Behavior of cyclopentane hydrates formation and dissociation in pure water and in the presence of sodium chloride*.
[32] Zylyftari, G., Ahuja, A., & Morris, J. F. (2014). Nucleation of cyclopentane hydrate by ice studied by morphology and rheology. *Chemical Engineering Science, 116*, 497-507.

[33] Aman, Z. (2012). Interfacial phenomena of cyclopentane hydrate. In C. A. Koh, A. K. Sum, M. Eberhart, G. Kubala, E. Sloan, & X. Yin (Eds.): ProQuest Dissertations Publishing.
[34] Nakajima, M., Ohmura, R., & Mori, Y. H. (2008). Clathrate Hydrate Formation from Cyclopentane-in-Water Emulsions. *Industrial & Engineering Chemistry Research, 47*(22), 8933-8939.
[35] Aliabadi, M., Rasoolzadeh, A., Esmaeilzadeh, F., & Alamdari, A. (2015). Experimental study of using CuO nanoparticles as a methane hydrate promoter. *Journal of Natural Gas Science and Engineering, 27*, 1518-1522.
[36] Liu, G.-Q., Wang, F., Luo, S.-J., Xu, D.-Y., & Guo, R.-B. (2017). Enhanced methane hydrate formation with SDS-coated Fe3O4 nanoparticles as promoters. *Journal of Molecular Liquids, 230*, 315-321.
[37] Su, Y., Bernardi, S., Searles, D. J., & Wang, L. (2016). Effect of Carbon Chain Length of Organic Salts on the Thermodynamic Stability of Methane Hydrate. *Journal of Chemical & Engineering Data, 61*(5), 1952-1960.
[38] Shu, B., Ma, X., Guo, K., & Li, J. (2004). Influences of different types of magnetic fields on HCFC-141b gas hydrate formation processes. *Science in China Series B: Chemistry, 47*(5), 428-433.
[39] Zhou, S., Zhang, J., Xu, T., Jiang, B., Xu, Y., & Wang, S. (2015). Progress in Research for the Factors of Promoting Natural Gas Hydrate Formation (in Chinese). *Petrochemical Technology, 44*(1), 127-132.
[40] Mali, G. A., Chapoy, A., & Tohidi, B. (2018). Investigation into the effect of subcooling on the kinetics of hydrate formation. *The Journal of Chemical Thermodynamics, 117*, 91-96.
[41] Arjmandi, M., Tohidi, B., Danesh, A., & Todd, A. C. (2005). Is subcooling the right driving force for testing low-dosage hydrate inhibitors? *Chemical Engineering Science, 60*(5), 1313-1321.
[42] Falabella, B. (1975). A STUDY OF NATURAL GAS HYDRATES. In: ProQuest Dissertations Publishing.
[43] Zhao, X., Qiu, Z., Huang, W., Zhou, G., & Zhang, Y. (2015). Inhibition mechanism and optimized design of thermodynamic gas hydrate inhibitors (in Chinese). *Acta Petrolei Sinica, 36*(6).
[44] Sa, J.-H., Kwak, G.-H., Han, K., Ahn, D., Cho, S. J., Lee, J. D., & Lee, K.-H. (2016). Inhibition of methane and natural gas hydrate formation by altering the structure of water with amino acids. *Scientific Reports, 6*, 31582.
[45] Bhattacharjee, G., Choudhary, N., Kumar, A., Chakrabarty, S., & Kumar, R. (2016). Effect of the amino acid l-histidine on methane hydrate growth kinetics. *Journal of Natural Gas Science and Engineering, 35*, 1453-1462.
[46] Veluswamy, H. P., Lee, P. Y., Premasinghe, K., & Linga, P. (2017). Effect of Biofriendly Amino Acids on the Kinetics of Methane Hydrate Formation and Dissociation. *Industrial and Engineering Chemistry Research, 56*(21), 6145-6154.
[47] Rahimi Mofrad, H., Ganji, H., Nazari, K., Kameli, M., Rezaie Rod, A., & Kakavand, M. (2016). Rapid formation of dry natural gas hydrate with high

capacity and low decomposition rate using a new effective promoter. *Journal of Petroleum Science and Engineering, 147*, 756-759.

[48] Ghozatloo, A., Hosseini, M., & Shariaty-Niassar, M. (2015). Improvement and enhancement of natural gas hydrate formation process by Hummers' graphene. *Journal of Natural Gas Science and Engineering, 27*(P2), 1229-1233.

[49] Wang, F., Meng, H. L., Guo, G., Luo, S. J., & Guo, R. B. (2017). Methane Hydrate Formation Promoted by -SO 3 - -coated Graphene Oxide Nanosheets. *ACS Sustainable Chemistry and Engineering, 5*(8), 6597-6604.

[50] Yan, S., Dai, W., Wang, S., Rao, Y., & Zhou, S. (2018). Graphene oxide: An effective promoter for CO 2 hydrate formation. *Energies, 11*(7).

[51] Firoozabadi, S. R., Bonyadi, M., & Lashanizadegan, A. (2018). Experimental investigation of Fe3O4 nanoparticles effect on the carbon dioxide hydrate formation in the presence of magnetic field. *Journal of Natural Gas Science and Engineering, 59*, 374-386.

[52] Chaplin, M. (2011). Water structure and science.

[53] Blandamer, M. J., Engberts, J. B. F. N., Gleeson, P. T., & Reis, J. C. R. (2005). Activity of water in aqueous systems; A frequently neglected property. *Chemical Society Reviews, 34*(5), 440-458.

[54] Sowa, B., Zhang, X., Hartley, P., Dunstan, D., Kozielski, K., & Maeda, N. (2014). Formation of Ice, Tetrahydrofuran Hydrate, and Methane/Propane Mixed Gas Hydrates in Strong Monovalent Salt Solutions. *Energy & Fuels, 28*(11), 6877-6888.

[55] Farhang, F., Nguyen, A. V., & Hampton, M. A. (2014). Influence of Sodium Halides on the Kinetics of CO2 Hydrate Formation. *Energy & Fuels, 28*(2), 1220-1229.

[56] Jager, M. D., Peters, C. J., & Sloan, E. D. (2002). Experimental determination of methane hydrate stability in methanol and electrolyte solutions. *Fluid Phase Equilibria, 193*(1), 17-28.

[57] Wang, W., Zhao, L., & Yan, B. (2010). Effects of Ions on Structure of Liquid Water (in Chinese). *Chemistry Bulletin*(6), 491-498.

[58] Zhang, J., Zhao, L., & Tan, X. (2004). Structural change of water clusters and the corresponding biological effects (in Chinese). *Chemistry, 67*(4), 278-278.

[59] Chen, J., Ye, S., Chen, S., Ye, Y., & Lv, F. (1995). Effects of electric field on water structure — research of electric field treated water on the application and mechanism (in Chinese). *Physics, 24*(7), 424-428.

[60] Szcześ, A., Chibowski, E., Hołysz, L., & Rafalski, P. (2011). Effects of static magnetic field on water at kinetic condition. *Chemical Engineering and Processing: Process Intensification, 50*(1), 124-127.

[61] Chang, K.-T., & Weng, C.-I. (2008). An investigation into the structure of aqueous NaCl electrolyte solutions under magnetic fields. *Computational Materials Science, 43*(4), 1048-1055.

[62] Jia, L., Li, Z., & Jia, S.-y. (2006). Applications of Magnetization Technology in the Treatment of Industrial Wastewater (in Chinese). *Chemical Industry and Engineering, 1*, 014.
[63] Hu, Y., Lee, B. R., & Sum, A. K. (2017). Universal correlation for gas hydrates suppression temperature of inhibited systems: I. Single salts. *AIChE Journal, 63*(11), 5111-5124.
[64] Hu, Y., Sa, J. H., Lee, B. R., & Sum, A. K. (2018). Universal correlation for gas hydrates suppression temperature of inhibited systems: III. salts and organic inhibitors. *AIChE Journal*, *64*(11), 4097-4109.
[65] NIST. (2017). Thermo Scientific NESLAB RTE-7 Circulating Bath-Specifications/Capabilities. Retrieved from https://www.nist.gov/laboratories/tools-instruments/thermo-scientific-neslab-rte-7-circulating-bath
[66] OMEGA®. (2018). 4-Channel RTD Input Data Acquisition Module with USB or Ethernet Interface. Retrieved from https://www.omega.com/en-us/communication-and-connectivity/data-acquisition-modules/p/PT-104A-Series
[67] OMEGA®. (2019). 4-Channel RTD Input Data Acquisition Module with USB or Ethernet Interface. Retrieved from https://www.omega.com/en-us/communication-and-connectivity/data-acquisition-modules/p/PT-104A-Series
[68] SDS, C. (2019). *Cyclopentane - Chemwatch Review Safety Data Sheet*.
[69] Aman, Z. M., Brown, E. P., Sloan, E. D., Sum, A. K., & Koh, C. A. (2011). Interfacial mechanisms governing cyclopentane clathrate hydrate adhesion/cohesion. *Phys. Chem. Chem. Phys., 13*(44), 19796-19806.
[70] SDS, C. (2019). *Sodium Chloride - Chemwatch Review Safety Data Sheet*.
[71] SDS, C. (2019). *Calcium Chloride - Chemwatch Review Safety Data Sheet*.
[72] SDS, C. (2019). *Aluminum Chloride - Chemwatch Review Safety Data Sheet*.
[73] Australia, N. P. (2016). Nulon Long Life Concentrated Coolant Safety Data Sheet. http://jr.chemwatch.net/CWWS/MaterialService.svc/GetMsdsByOldExternalUrl?&mode=SAP&passop=checkpass&user=nulon&pwd=MSDS000&cwno=86497&msdsformat=GHS&db=own&onlyfirst=1
[74] Australia, N. P. (2016). Green Premium Long Life Coolant 100% Concentrate. Retrieved from https://www.nulon.com.au/products/cooling-systems/green-premium-long-life-coolant-100-percent-concentrate
[75] UQ. (2019). *Alcoholic Hydroxide Solutions Preparation Notes*.
[76] Irvine, U. (2019). Alcohol-hydroxide cleaner INRF Application Note. Retrieved from https://www.inrf.uci.edu/wordpress/wp-content/uploads/sop-wet-alcohol-hydroxide-cleaner.pdf
[77] Scientific™, F. (2019). Fisherbrand™ Traceable™ Memory-Loc™ Datalogging Thermometers. Retrieved from

https://www.fishersci.com/shop/products/fisher-scientific-traceable-memory-loc-datalogging-thermometers-7/p-4700743
[78] LIU, G.-q., MA, L.-x., & LIU, J. (2002). Handbook of substances properties data in chemical and engineering (inorganic Vol)(化学化工物性数据手册)(无机卷). In: Beijing (北京): Chemical Industry Press (化学工业出版社).
[79] CO., W. H. C. (2014). Degrees Baumé of Calcium Chloride Solution in Different Mass Fraction.
[80] Sun, Z., Liu, C., & Huang, H. (2012). *Experimental Study on Cyclopentane Hydrate Formation.*
[81] Wu, R. Z. J. (2014). *Experimental Studies of Gas Hydrate Formation.* University of Western Australia,
[82] Ho-Van, S., Bouillot, B., Douzet, J., Babakhani, S. M., & Herri, J. M. (2018). Implementing Cyclopentane Hydrates Phase Equilibrium Data and Simulations in Brine Solutions. *Industrial and Engineering Chemistry Research, 57*(43), 14774-14783.
[83] LibreTexts™. (2019). Freezing Point Depression. Retrieved from https://chem.libretexts.org/Bookshelves/Physical_and_Theoretical_Chemistry_Textbook_Maps/Supplemental_Modules_(Physical_and_Theoretical_Chemistry)/Physical_Properties_of_Matter/Solutions_and_Mixtures/Colligative_Properties/Freezing_Point_Depression
[84] Wikipedia. (2019). van 't Hoff factor. Retrieved from https://en.wikipedia.org/wiki/Van_%27t_Hoff_factor
[85] LibreTexts™. (2019). 13.9: Solutions of Electrolytes. Retrieved from https://chem.libretexts.org/Bookshelves/General_Chemistry/Map%3A_General_Chemistry_(Petrucci_et_al.)/13%3A_Solutions_and_their_Physical_Properties/13.09%3A_Solutions_of_Electrolytes
[86] Corak, D., Barth, T., Høiland, S., Skodvin, T., Larsen, R., & Skjetne, T. (2011). Effect of subcooling and amount of hydrate former on formation of cyclopentane hydrates in brine. *Desalination, 278*(1), 268-274.
[87] LibreTexts™. (2019). 5.8: Ionic Activity. Retrieved from https://chem.libretexts.org/Bookshelves/Physical_and_Theoretical_Chemistry_Textbook_Maps/Map%3A_Physical_Chemistry_for_the_Biosciences_(Chang)/05%3A_Solutions/5.08%3A_Ionic_Activity
[88] Debye, P., & Hückel, E. (1923). The theory of electrolytes: I. lowering of freezing point and related phenomena. *Physikalische Zeitschrift., 24*, 185-206.
[89] Zylyftari, G., Lee, J., & Morris, J. (2013). Salt effects on thermodynamic and rheological properties of hydrate forming emulsions. *Chemical Engineering Science, 95*, 148-160.
[90] Kishimoto, M., Iijima, S., & Ohmura, R. (2012). Crystal Growth of Clathrate Hydrate at the Interface between Seawater and Hydrophobic-

Guest Liquid: Effect of Elevated Salt Concentration. *Industrial & Engineering Chemistry Research, 51*(14), 5224-5229-5224-5229.

APPENDIX-A Proven Natural Gas Reserves over the World

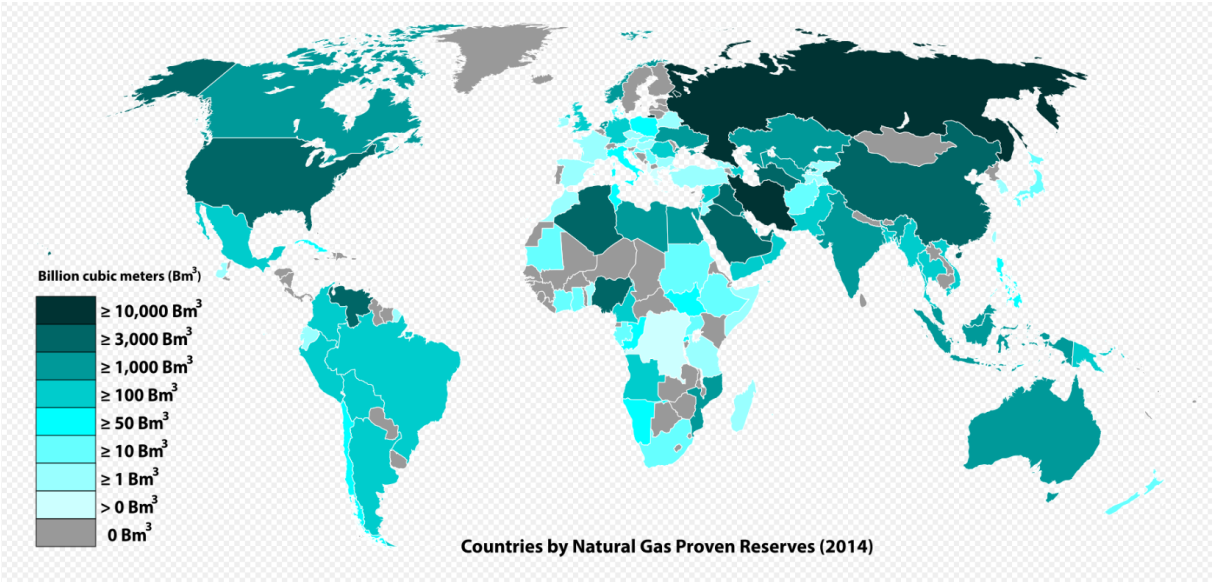

Figure 36 Proven Natural Gas Reserves (2014)

APPENDIX-B Summarized Equilibrium Temperature at Different Molality

Table 18 Measured Equilibrium Temperatures at Different Molality

Approximate Value of Molality (mol/kg H_2O)	Equilibrium Temperature @Different Molality of Electrolyte (℃)		
	NaCl Solution	$CaCl_2$ Solution	$AlCl_3$ Solution
0	7.7	7.7	7.7
0.10	-*	-*	6.953
0.20	-*	6.725	6.750
0.35	-*	-*	6.401
0.50	6.126	5.365	5.605
0.70	5.030	4.738	4.397
1.00	4.378	2.647	-*
1.50	2.532	-*	-*
* Unmeasured Data			

APPENDIX-C Graphs of Estimating NaCl and $CaCl_2$ Freezing Points

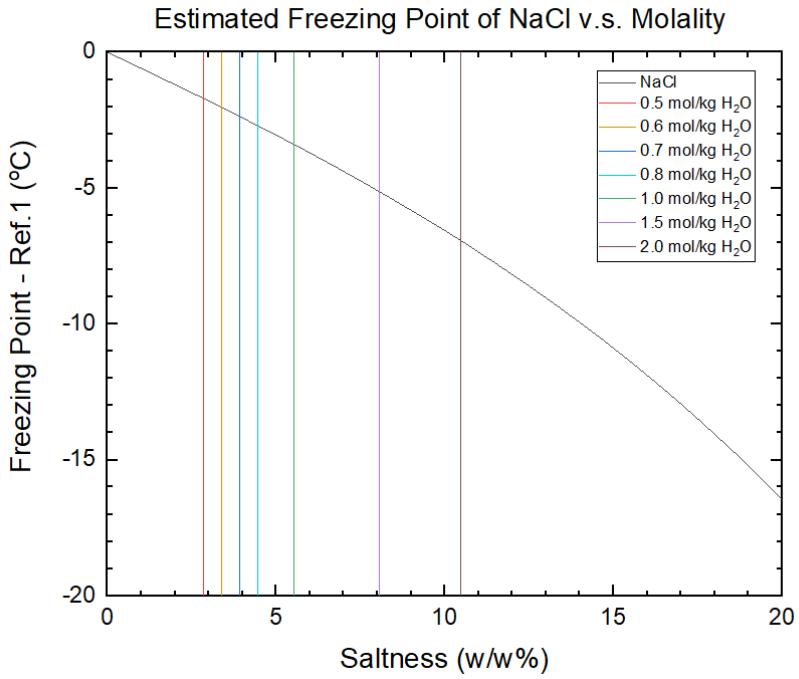

Figure 37 Estimated Freezing Point of NaCl (Based on Ref.1: Liu et al., 2002)

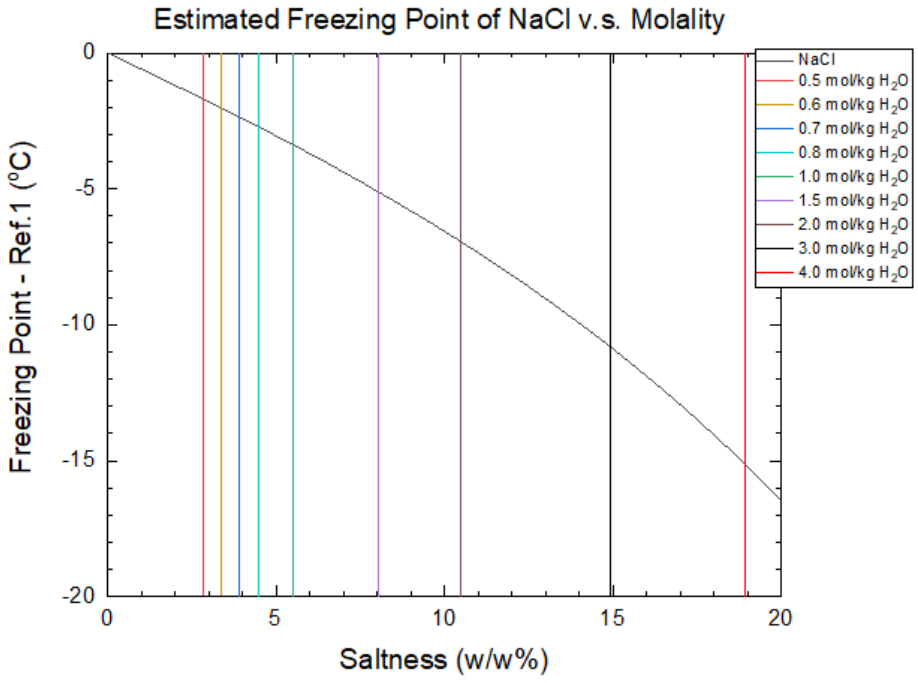

Figure 38 Estimated Freezing Point of $CaCl_2$ (Based on Ref.1: Liu et al., 2002)

APPENDIX-D Effective Mole Fraction Calculation

Based on Equation 2,

$$X = \sum_{j=salts} \sum_{i=ions} |z_{j,i}| x_{j,i}$$

The effective mole fraction can be calculated with the designed molality.

For NaCl solution,

$$X_{\mathrm{NaCl}} = \frac{b_{\mathrm{NaCl}} \times (|+1| \times 1 + |-1| \times 1)}{b_{\mathrm{NaCl}} \times (1+1) + n_{\mathrm{water}}} = \frac{2b_{\mathrm{NaCl}}}{2b_{\mathrm{NaCl}} + n_{\mathrm{water}}}$$

$$= \frac{1}{1 + \frac{n_{\mathrm{water}}}{2b_{\mathrm{NaCl}}}}$$

For $CaCl_2$ solution,

$$X_{\mathrm{CaCl_2}} = \frac{b_{\mathrm{CaCl_2}} \times (|+2| \times 1 + |-1| \times 2)}{b_{\mathrm{CaCl_2}} \times (1+2) + n_{\mathrm{water}}} = \frac{4b_{\mathrm{CaCl_2}}}{3b_{\mathrm{CaCl_2}} + n_{\mathrm{water}}}$$

$$= \frac{1}{\frac{3}{4} + \frac{n_{\mathrm{water}}}{4b_{\mathrm{CaCl_2}}}}$$

For $AlCl_3$ solution,

$$X_{\mathrm{AlCl_3}} = \frac{b_{\mathrm{AlCl_3}} \times (|+3| \times 1 + |-1| \times 3)}{b_{\mathrm{AlCl_3}} \times (1+3) + n_{\mathrm{water}}} = \frac{6b_{\mathrm{AlCl_3}}}{4b_{\mathrm{AlCl_3}} + n_{\mathrm{water}}}$$

$$= \frac{1}{\frac{2}{3} + \frac{n_{\mathrm{water}}}{6b_{\mathrm{CaCl_2}}}}$$

b_{NaCl}, $b_{\mathrm{CaCl_2}}$, and $b_{\mathrm{AlCl_3}}$ are the molality of salt solutions;

$n_{\mathrm{water}} \approx 55.56$ mol for 1 kg water.

APPENDIX-E Mass Fraction Calculation

Based on Equation 6,

$$\omega = \frac{b \times \mathrm{MW}_{salt}}{(b \times \mathrm{MW}_{salt} + 1000)} \times 100\%$$

The mass fraction can be calculated with the designed molality.

For NaCl solution,

$$\omega_{\mathrm{NaCl}} = \frac{b_{\mathrm{NaCl}} \times 58.44}{(b_{\mathrm{NaCl}} \times 58.44 + 1000)} \times 100\%$$

For $CaCl_2$ solution,

$$\omega_{\mathrm{CaCl_2}} = \frac{b_{\mathrm{CaCl_2}} \times 110.99}{\left(b_{\mathrm{CaCl_2}} \times 110.99 + 1000\right)} \times 100\%$$

For $AlCl_3$ solution,

$$\omega_{\mathrm{AlCl_3}} = \frac{b_{\mathrm{AlCl_3}} \times 133.3}{\left(b_{\mathrm{AlCl_3}} \times 133.3 + 1000\right)} \times 100\%$$

b_{NaCl}, $b_{\mathrm{CaCl_2}}$, and $b_{\mathrm{AlCl_3}}$ are the molality of salt solutions.

APPENDIX-F Ionic Strength Calculation

Based on Equation 10Equation 2,

$$I = \frac{1}{2}\sum_{i}^{n} c_i {z_i}^2$$

The effective mole fraction can be calculated with the designed molality.

For NaCl solution,

$$I_{\mathrm{NaCl}} = \frac{1}{2} b_{\mathrm{NaCl}} \times (1 \times |+1|^2 + 1 \times |-1|^2) = b_{\mathrm{NaCl}}$$

For $CaCl_2$ solution,

$$I_{\mathrm{CaCl_2}} = \frac{1}{2} b_{\mathrm{CaCl_2}} \times (1 \times |+2|^2 + 2 \times |-1|^2) = 3b_{\mathrm{CaCl_2}}$$

For $AlCl_3$ solution,

$$I_{\mathrm{AlCl_3}} = \frac{1}{2} b_{\mathrm{AlCl_3}} \times (1 \times |+3|^2 + 3 \times |-1|^2) = 6b_{\mathrm{AlCl_3}}$$

b_{NaCl}, $b_{\mathrm{CaCl_2}}$, and $b_{\mathrm{AlCl_3}}$ are the molality of salt solutions.

APPENDIX-G Relationship between Effective Mole Fraction and Ionic Strength

For NaCl solution,

From APPENDIX-D

$$X_{\mathrm{NaCl}} = \frac{2b_{\mathrm{NaCl}}}{2b_{\mathrm{NaCl}} + n_{\mathrm{water}}}$$

and APPENDIX-F

$$I_{\mathrm{NaCl}} = b_{\mathrm{NaCl}}$$

the relationship between effective mole fraction and ionic strength is

$$X_{\mathrm{NaCl}} = \frac{2I_{\mathrm{NaCl}}}{2I_{\mathrm{NaCl}} + n_{\mathrm{water}}}$$

that is,

$$\frac{1}{X_{\mathrm{NaCl}}} = 1 + \frac{n_{\mathrm{water}}}{2} \times \frac{1}{I_{\mathrm{NaCl}}}$$

Thus, a linear correlation exists between the reciprocal of effective mole fraction and the reciprocal of ionic strength.

The relationship between effective mole fraction and ionic strength can be considered as linear, when the factor $2I_{\mathrm{NaCl}}$ in the denominator is neglected. Because the value of this factor is relatively low compared with the mole of 1 kg DI water.

Then,

$$X_{\mathrm{NaCl}} = \frac{2I_{\mathrm{NaCl}}}{n_{\mathrm{water}}}$$

The calculation error is about 5%, when b_{NaCl}=1.50 mol/kg H_2O.

Similarly, for $CaCl_2$ solution,

$$X_{CaCl_2} = \frac{4b_{CaCl_2}}{3b_{CaCl_2} + n_{water}}$$

$$I_{CaCl_2} = 3b_{CaCl_2}$$

Thus,

$$X_{CaCl_2} = \frac{\frac{4}{3}I_{CaCl_2}}{I_{CaCl_2} + n_{water}} = \frac{4I_{CaCl_2}}{3I_{CaCl_2} + 3n_{water}}$$

$$\frac{1}{X_{CaCl_2}} = \frac{3}{4} + \frac{3n_{water}}{4} \times \frac{1}{I_{CaCl_2}}$$

Then,

$$X_{CaCl_2} = \frac{4I_{CaCl_2}}{3n_{water}}$$

The calculation error is about 5%, when b_{CaCl_2}=1.0 mol/kg H_2O.

Similarly, for $AlCl_3$ solution,

$$X_{AlCl_3} = \frac{6b_{AlCl_3}}{4b_{AlCl_3} + n_{water}}$$

$$I_{AlCl_3} = 6b_{AlCl_3}$$

Thus,

$$X_{AlCl_3} = \frac{I_{AlCl_3}}{\frac{2}{3}I_{AlCl_3} + n_{water}} = \frac{3I_{AlCl_3}}{2I_{AlCl_3} + 3n_{water}}$$

$$\frac{1}{X_{AlCl_3}} = \frac{2}{3} + n_{water} \times \frac{1}{I_{AlCl_3}}$$

Then,

$$X_{AlCl_3} = \frac{I_{AlCl_3}}{n_{water}}$$

The calculation error is about 5%, when b_{CaCl_2}=0.71 mol/kg H_2O.